Interplay Between Wind-Driven Advection and Mixing of Salt and Dissolved Oxygen in a Microtidal Estuary

Jianxing Wang[1], Johanna H. Rosman[1], James L. Hench[2], Nathan S. Hall[1], Anthony C. Whipple[1], Richard A. Luettich, Jr[1]

[1]Institute of Marine Sciences, University of North Carolina at Chapel Hill, Morehead City, NC, USA

[2]Marine Laboratory, Nicholas School of the Environment, Duke University, Beaufort, NC, USA

Key Points

1. In shallow estuaries with small tides, wind-driven currents and mixing interact to control stratification and bottom oxygen concentrations

2. For cross- and up-estuary winds advection decreases stratification and turbulence is increased, leading to a well-mixed water column

3. For down-estuary wind the water column becomes stratified or well-mixed depending on the balance of advection and enhanced turbulence

Abstract

Most work on how estuarine dynamics impact dissolved oxygen (DO) distributions has focused on tides as the primary mixing mechanism, but in shallow estuaries with large fetch or small tides, wind can be the primary mixing agent and also drives advection. To investigate how these processes interact and affect DO distributions, an observational study was conducted in the shallow, micro-tidal Neuse Estuary (NRE). Salinity, DO, and velocity profiles were measured at multiple positions along and across the estuary over a 6-month period. A one-dimensional model (General Ocean Turbulence Model) provided additional insight into the response of salinity and DO to wind. Salinity and oxygen conservation equation terms were calculated from observations and simulations to investigate the roles of advection and mixing under different conditions. Cross-estuary wind drove lateral circulations and tilted the isohalines, reducing stratification; lateral advection and enhanced vertical mixing reduced vertical gradients and increased the bottom DO. Down-estuary wind tended to increase the exchange flow and increase stratification, but concurrently the wind-driven surface turbulent boundary layer deepened over time. The balance of these processes determined if the water column became fully mixed or remained stratified, and the depth of the pycnocline and oxycline. Up-estuary wind inhibited the exchange flow and ultimately the combination of advection and vertical mixing homogenized the water column. While these patterns generally held for purely across- or along-channel wind, the response was often more complex because the wind vector could have any orientation and wind speed and direction varied continuously with time.

Plain Language Summary

Dissolved oxygen (DO) is fundamental for marine ecosystems and can be depleted when consumption in the sediment and water column exceeds replenishment by exchange with the atmosphere and vertical mixing. Estuaries with small tides often have problems with low DO near the bottom because turbulence is insufficient to mix the water column. In these estuaries, wind is important for driving currents and mixing, both of which affect vertical salinity gradients (stratification) and DO. We investigated wind effects on stratification and DO using measurements in the Neuse Estuary, which has very small tides, together with a simplified model. We found that wind blowing across the estuary or toward upstream mixes the water column and oxygenates the bottom water. Wind blowing toward downstream generally enhances downstream current in the upper layer and upstream current in the lower layer which brings more salty ocean water into the estuary, increases stratification, and leads to low bottom DO. However, if the wind is strong enough it can generate enough turbulence to fully mix the water column and increase bottom DO. Further research is needed to understand how real wind, which can come from any direction and varies with time, affects stratification and DO in estuaries.

1 Introduction

Dissolved oxygen (DO) is fundamental for marine ecosystems and constrains ocean productivity, biodiversity and biogeochemical cycles [*Breitburg et al.*, 2018]. Oxygen level has been decreasing in many coastal waters since the mid-1900s and the hypoxia occurrences ([O_2]< 2 mg/L, also termed dead zones) have been doubling each decade [*R. J. Diaz*, 2001; *R.J. Diaz and Rosenberg*, 2008; *Keeling et al.*, 2010]. Anthropogenic nutrient loads and climate change are considered two major causes. Over 2 °C temperature increase was found in most dead zones by the end of the 20th century [*Altieri and Gedan*, 2015]. A 43% increase in riverine nitrogen fluxes between 1970 and 2000 happened in the coastal waters, causing eutrophication, dramatically stimulating primary production and inducing harmful algal blooms (HAB) and depleting oxygen [*Reed and Harrison*, 2016]. Although it is widely acknowledged that the increase of nutrient loads leads to an increase in the severity of hypoxia, correlating nutrient loads to interannual variations in hypoxic volume often fails to explain the majority of the variability [*Hagy et al.*, 2004; *Scully*, 2010a]. Also, substantial reductions in nutrient loads have been made along many coasts, but oxygen levels have not met expectations and have continued to decline [*Lee and Lwiza*, 2008; *Riemann et al.*, 2015]. A deeper understanding of the mechanisms of hypoxia is therefore needed.

Hypoxia happens when biological consumption through respiration exceeds the rate of oxygen supplied by physical transport, air-sea fluxes and photosynthesis for sufficient periods of time [*Breitburg et al.*, 2018]. In estuarine and coastal areas, physical processes including vertical mixing and circulation patterns influence horizontal and vertical transport of DO. Stratification is considered a major cause of bottom hypoxia as it inhibits turbulence mixing and downward diffusion of DO from surface to bottom layers [*Cui et al.*, 2019; *Officer et al.*, 1984].

Wind forcing is known to affect estuarine circulation and stratification, especially in micro-tidal estuaries [*Li and Li*, 2012; *Sanford and Chen*, 2009; *M.E. Scully et al.*, 2005; *Xie and Li*, 2018]. Previously, wind stress was considered to be predominantly a source of energy that caused mixing and reduced estuarine stratification [*Simpson and Bowers*, 1981; *Simpson et al.*, 1991]. Scully et al. (2005) demonstrated that the along-channel wind plays an important role in governing the strength of the estuarine exchange flow and the corresponding increase or decrease in stratification. Sanford and Chen (2009) showed that up-estuary wind (wind directed toward up-estuary) tends to inhibit the exchange flow and decrease the stratification while down-estuary wind first increases then decreases the exchange flow and stratification. Such a transition results from the competition between wind straining and wind mixing. Wind straining is an increase or decrease in stratification caused by differential horizontal advection of salt in the upper and lower water column due to vertical shear in the wind-driven current. Wind stress also generates a turbulent boundary layer that grows downward with time and can erode stratification [*Kato and Phillips*, 2006]. Wind straining dominates over wind mixing under moderate down-estuary wind but is quickly overcome by the wind mixing when the wind becomes strong [*Sanford and Chen*, 2009]. Li and Li (2012) found from simulations that along-estuary wind could also drive lateral circulation due to the Coriolis effect, thereby tilting isopycnals and decreasing stratification.

Through affecting the estuarine circulation and stratification, the wind can further influence the DO dynamics and hypoxia events [*Cui et al.*, 2019; *Lee and Lwiza*, 2008; *Malcolm E. Scully*, 2010b; 2013]. Scully (2013) found that wind speeds and directions have a large impact on the seasonal cycle of hypoxia in Chesapeake Bay. Scully (2010b) showed that the wind-driven lateral circulation driven by the Coriolis effect in combination with along-channel wind, and enhanced vertical mixing due to the decrease of the stratification are two dominant mechanisms for providing oxygen to the bottom water.

For at least the past several decades, the Neuse River Estuary (NRE) has been experiencing hypoxia/ anoxia events frequently, especially in summer. Severe eutrophication due to anthropogenic nutrient loading provides a seasonal burst of organic matter supply to bottom waters in spring and summer and a legacy of organic rich sediments. In combination with vertical density stratification, the resultant high oxygen demand leads to bottom hypoxia [*Katin et al.* 2019]. Stronger stratification is found to exacerbate the hypoxia [*Buzzelli et al.*, 2002b]. In the upper NRE, cross-channel wind has been observed to drive lateral circulations and upwell bottom low DO and high salinity water [*Reynolds-Fleming and Luettich*, 2004]. However, a quantitative understanding of wind effects on salinity and DO dynamics is needed.

This paper describes a combined observational and modeling study in the NRE to investigate wind effects (including speeds and directions) on salinity and DO dynamics in estuaries. Cross-channel, up-estuary and down-estuary wind events in the field observations are used to qualitatively and quantitatively describe the impacts of wind direction and speed on salinity and DO distributions. Dominant mechanisms controlling the salinity and DO distributions under different wind conditions are assessed using salinity and DO budgets based on observational data and 1-D model simulations.

2 Methods

2.1 Study Site

The Neuse River Estuary (NRE) is a 73 km-long estuary that connects with the Pamlico Sound. The estuary bends ~90 degrees at Minnesott Beach, which separates it into an upper part oriented roughly NW-SE and a lower part oriented roughly SW-NE (Figure 1). The NRE is characterized as a shallow (averaged depth <4 m), microtidal (tidal range < 30 cm), river-dominated estuary

[*Luettich et al.*, 2000]. Wind, therefore, is important for driving the mixing and circulation in the NRE [*Rizzo and Christian*, 1996]. The NRE varies from vertically well-mixed to highly stratified depending on the wind, and density stratification in the NRE is controlled mainly by salinity gradients, which are dynamically much more significant than the temperature gradients [*Whipple et al., 2006*].

2.2 Field measurements

Three sets of field observations were used in this study: (1) time series of velocity and water quality parameter profiles from moorings at a central site (AVP site), (2) shipboard observations of velocity and water quality parameter profiles at stations along three cross-estuary transects, and (3) shipboard observations of water quality parameters at stations along the estuary collected as part of the MODMON program (Figure 1).

The AVP site was at the center of the lower NRE and was the focus site for the analysis. An Autonomous Vertical Profiler (AVP) was deployed in the middle of the estuary channel to measure profiles of salinity, temperature and dissolved oxygen (DO) from May 16th to Oct. 4th, 2016. The AVP is a floating platform that lowers a CTD (EXO2 Sonde, YSI) through the water column [*Reynolds-Fleming et al.*, 2002; *Whipple et al.*, 2006]. The CTD was lowered at a constant rate of 0.01 m/s from the surface to 6 m depth at 30-min intervals. An anemometer on the AVP platform measured the wind speed and direction 5 m above the water surface, also at 30-min intervals. A CTD chain adjacent to the AVP that contained three SBE37-SMP-ODO CTDs (1, 2.85 and 4.71 m above seabed) was deployed to verify calibration of the Sonde on the AVP. An upward-looking acoustic Doppler current profiler (ADCP, Teledyne-RD Instruments 1.2-MHz Workhorse Monitor) mounted at the bottom (0.63 m above the seabed) adjacent to the AVP measured velocity profiles in 0.25-m vertical bins at 5-min intervals.

To measure the structure of salinity, DO and velocity across the estuary, shipboard measurements were made along transects at the mouth, middle of the lower Neuse, and bend. There were 10 - 12 equally spaced stations (500 m apart) on each cross-estuary transect. Shipboard measurements were collected at each station once a day (around noon) on 8 days (8 and 20 June, 5 and 18 July, 3 and 16 August, 7 and 19 September 2016). At each station, velocity profiles were measured with a boom-mounted ADCP for six minutes in mode 1, with 0.25 m bins. CTD casts (SBE19plus V2, Seabird Electronics) were made at each station with a sampling rate of 4 Hz to measure salinity, temperature and DO profiles.

This study also utilized measurements from the Neuser River Estuary Modeling and Monitoring program (ModMon) [*Luettich et al.*, 2000]. The ModMon dataset includes vertical profiles of temperature, salinity, and DO measured biweekly at stations along the main channel of the NRE. ModMon data are publicly available and can be accessed through the Southeast Coastal Ocean Observing Regional Association's data portal at https://portal.secoora.org/.

2.3 Salinity and Oxygen Budget Calculations

Salinity and oxygen budgets were analyzed by calculating terms of the conservation equations from the field measurements. Vertical advection and horizontal mixing were assumed to be negligible compared with other terms. The conservation equation for salinity is

$$\frac{\partial S}{\partial t} = \frac{\partial}{\partial z}\left(K_z \frac{\partial S}{\partial z}\right) - u\frac{\partial S}{\partial x} - v\frac{\partial S}{\partial y} \qquad (1)$$

where S is the salinity, u and v are the along-channel and cross-channel velocities, and K_z is the vertical eddy diffusivity. The first term on the right is the vertical mixing and the second and third terms are along-channel and cross-channel advection.

The conservation equation for dissolved oxygen is

$$\frac{\partial C_{O_2}}{\partial t} = \frac{\partial}{\partial z}\left(K_z \frac{\partial C_{O_2}}{\partial z}\right) - u\frac{\partial C_{O_2}}{\partial x} - v\frac{\partial C_{O_2}}{\partial y} + P \qquad (2)$$

where the first term on the right is the vertical mixing of oxygen, the second and third terms are the along-channel and cross-channel advection and the fourth term represents production and respiration by phytoplankton. The expression used for *P* is [*Jassby and Platt*, 1976]

$$P = PQ\,\frac{32}{12}\,C_{chl}\left(P_{max}\,\tanh\frac{\alpha I_z}{P_{max}} - R\right) \qquad (3)$$

$$R = 0.1\,P_{max} \qquad (4)$$

where the PQ is photosynthetic quotient for phytoplankton growing on ammonium [*Oviatt et al.*, 1986; *Smith et al.*, 2012], C_{chl} is the concentration of chlorophyll *a* in the water and a typical value is used (Table 1), P_{max} is the average chlorophyll *a* specific light saturated photosynthetic rate and *α* is the average slope of the light-limited region of the *P* versus irradiance relationship [*Buzzelli et al.*, 2002a]. I_z is the irradiance at the depth z below the water surface based on Beer's law:

$$I_z = I_o\, e^{K_d * z} \qquad (5)$$

where I_o is the incident irradiance:

$$I_o = \begin{cases} -I_{max}\cos 2\pi t\,, & \cos 2\pi t < 0 \\ 0, & \cos 2\pi t \geq 0 \end{cases} \qquad (6)$$

t is time in days (*t* = 0 is midnight). I_{max} is the maximum irradiance at the surface. K_d in Eq. 5 is the extinction coefficient for photosynthetically active radiation, and *z* is the depth below the water surface. R is the respiration rate of the phytoplankton and it is set as 10% of the P_{max} (Eq. 4). The values of parameters from Eq. 3 to Eq. 6 are shown in Table 1.

Every term in Eq. 1 and Eq. 2 was calculated at the AVP station except the mixing term because K_z was not known. The along-estuary gradients, $\frac{\partial S}{\partial x}$ and $\frac{\partial C_{O_2}}{\partial x}$, were calculated based on the AVP and two adjacent MODMON stations (station 140 and 180 shown in Figure 1). The across-estuary gradients, $\frac{\partial S}{\partial y}$ and $\frac{\partial C_{O_2}}{\partial y}$, were calculated based on the AVP and two adjacent central transect shipboard stations (station 5 and 7). The horizontal velocity measured by the bottom-mounted ADCP was decomposed into along-channel (x) and cross-channel (y) components (u, v). The major axis of the depth-averaged velocity from the 6-month dataset was used to define the along-channel direction (positive seaward).

2.4 Idealized Simulations

Idealized simulations were used to investigate the role of turbulent mixing for the salinity and DO dynamics, and compare salinity and DO budgets with the observations. The General Ocean Turbulence Model (GOTM) was used to simulate the evolution of velocity and salinity profiles, and turbulence properties under different wind conditions. GOTM is a 1-dimensional (vertical) model that solves the transport equations of momentum, salt and heat [*Umlauf et al.*, 2005]. It contains multiple well-tested turbulence models that are widely used [*Ladwig et al.*, 2021; *Lange and Burchard*, 2019].

The model setup was based on the observation data, with a depth of 6.3 m and initial salinity and temperature profiles from June 20th. The model was initialized by setting velocity, vertical eddy viscosity and diffusivity to zero. The vertical eddy viscosity and diffusivity were calculated by the Mellor-Yamada (M-Y) turbulence closure model with the stability function proposed by Schumann et al. [*Mellor and Yamada*, 1982; *Schumann and Gerz*, 1995]. The bottom roughness (z_0) was calculated based on a log fit to velocity profiles measured with downward-looking current profiler (Nortek Aquadopp-HR) near the AVP station that measured in high resolution (pulse coherent) mode. Constant along-channel and lateral salinity gradients ($\frac{\partial s}{\partial x}, \frac{\partial s}{\partial y}$) from the data were used. The model was forced by winds (Table 2) and a constant river inflow (0.01 m/s) with no tide or Coriolis force. Wind stress was calculated from wind velocity with a constant drag coefficient (C_d) [*Blanton et al.*, 1989]. Down-estuary, up-estuary and cross-estuary wind events were simulated to investigate wind effects on salinity and oxygen budgets. For down-estuary winds, simulations were run for three wind speeds (5, 10, 15 m/s) to investigate the implications for wind straining and wind mixing. For up-estuary winds and cross-channel winds, the wind speed was 5 m/s. In the along-channel wind cases, the cross-estuary salinity gradient $\frac{\partial s}{\partial y}$ was set as zero. Every simulation ran for 60 hours (started from midnight) but the 10 m/s down-estuary wind scenario ran for 1 month to capture the final steady state. Values used for parameters are shown in Table 2.

Evolution of dissolved oxygen profiles was calculated by solving the conservation equation for dissolved oxygen. Velocity, temperature and eddy diffusivity profiles from GOTM output were used. Along-channel and lateral oxygen gradients ($\frac{\partial c_{O_2}}{\partial x}, \frac{\partial c_{O_2}}{\partial y}$) were set to constant values based on observations. The lateral oxygen gradient ($\frac{\partial c_{O_2}}{\partial y}$) was set as zero for the along-channel wind events. The air-sea oxygen exchange was included as a flux boundary condition at the water surface. The expression of air-sea oxygen flux is [*Wanninkhof et al.*, 2009]:

$$ASX = k\, k_o\, \Delta P_{O_2} \qquad (7)$$

where the k is the piston velocity and k_o is Henry's constant. ΔP_{O_2} is the difference of partial pressures of oxygen between the air and water. The expression for k is:

$$k = k_{600} {\frac{S_c}{600}}^{-0.5} \qquad (8)$$

where the k_{600} is the piston velocity of CO_2 and the S_c is the Schmidt number for oxygen based on Wanninkhof et al. (2009). The sediment oxygen demand (SOD) was applied as a flux at the bottom boundary and considered a constant (25 mmol/(m^2*d)) based on observations from previous studies [*Luettich Jr et al.*, 2000]. The production and respiration term was calculated based on equation 3 with the values of parameters shown in Table 1. The conservation equation for dissolved oxygen (Eq. 2) was solved using a forward differencing scheme in MATLAB.

3 Results

3.1 Overview of Field Observations

During the 6-month observation period, there were general relationships between wind, stratification strength and bottom DO. In June and September, the wind was mostly in the NE (toward north shore)-SW (toward south shore) directions (Figure 2a and 2c) and had both an along-channel and cross-channel component in the lower Neuse. During July and August, there was strong variability in wind speed and direction at diurnal frequencies due to the sea breeze. Stratification, expressed as salinity difference between surface and bottom (ΔS), generally correlated with the along-channel wind, increasing with down-estuary wind and decreasing with up-estuary wind. Bottom DO was inversely corelated with the along-channel wind or the ΔS, decreasing during down-estuary wind when the water column was more stratified and increasing during up-estuary wind when the water column was more mixed. Bottom DO was almost completely depleted (anoxic) in the observed area for about a month from July 18^{th} to Aug. 28^{th} under the continuous moderate down-estuary wind condition and finally rose when the wind switched to up-estuary direction for about three days after Aug. 28^{th} (Figure 2c and 2d).

Two days were selected from the 6-month dataset to study the wind effects on the salinity and DO dynamics: June 20th to June 21st at noon and Sept. 19th (Figure 3 and 4) because they contained significant wind events oriented in along-channel and cross-channel directions of sufficient duration, and because all the datasets contained data for these days. On June 20th, the wind blew south-eastward, cross-channel toward the south shore during the first half of the day and switched to a north-eastward, down-channel direction during the latter half of June 20th into June 21st (Figure 3a). On Sept. 19th, the wind blew north-westward, cross-channel toward the north shore, during the first half and turned to south-westward toward up-channel direction during the latter half (Figure 4a).

On June 20th, when the wind was directed across the estuary during the first half of the day, a clockwise lateral circulation was observed with a maximum speed of 0.21 m/s (Figure 3c, 5a). Surface fresher water was advected to the south shore and bottom saltier water to the north shore. The halocline, therefore, was tilted and the stratification was decreased. Bottom low DO water was also pushed to the north shore (Figure 5c). As the down-estuary component of the wind increased, the exchange flow strengthened and the surface outflow layer deepened (Figure 3b). A high salinity layer was formed at first at the bottom as a result of the increase of the exchange flow (Figure 3d). Dissolved oxygen concentrations in this layer were very low (DO < 2mg/L, Figure 3e). With the increase of the wind speed, the halocline deepened and finally disappeared at noon on June 21st at which time the water columnwas well-mixed. The low DO layer also decreased in thickness and disappeared when the water column became well-mixed. After midnight, the exchange flow began to decrease and disappeared in several hours, possibly due to establishment of barotropic (water surface slope) and baroclinic pressure gradients (isopycnal tilt) that balanced the wind stress.

On Sept. 19th, the wind first blew toward the north shore (Figure 4a) resulting in clockwise lateral circulation with maximum speed of about 0.2 m/s (Figure 4c). Surface fresher water was pushed to the north shore and bottom saltier water to the south shore, the halocline was tilted and stratification decreased (Figure 5b). Following the salinity, bottom low DO water was pushed to the south shore (Figure 5d). The up-estuary wind started to blow from about 18:00 and continued to increase to a maximum speed of 12 m/s (Figure 4a). The exchange flow was initially reversed, with upstream flow at the surface and downstream flow near the bottom (Figure 4b). Salinity stratification decreased with time until the water became well-mixed (Figure 4d). After the salinity became uniform over the water depth, the velocity was up-estuary over the entire water column. As stratification decreased, the DO in the bottom layer increased from about 3 mg/L to 5.5 mg/L when the water column became well-mixed (Figure 4e).

3.2 Salinity and DO Budgets from Observations

Terms of the salinity and DO budget equations were calculated from field observations for cross-channel wind events (black dashed lines in Figures 3 and 4) and at night for along-channel wind events on both days (black dotted lines in Figures 3 and 4). Along-channel and cross-channel gradients of salinity and DO ($\frac{\partial S}{\partial x}$, $\frac{\partial C_{O_2}}{\partial x}$, $\frac{\partial S}{\partial y}$ and $\frac{\partial C_{O_2}}{\partial y}$) were only measured during the daytime, during the period when wind was across channel; therefore, advection terms were only calculated for cross-channel wind events. Vertical mixing terms were not calculated because the vertical eddy diffusivity (K_z) was not known. Thus, the time rate of changes of salinity and DO ($\frac{\partial S}{\partial t}$, $\frac{\partial C_{O_2}}{\partial t}$), longitudinal and lateral advections of salinity and DO ($-u\frac{\partial S}{\partial x}$, $-v\frac{\partial S}{\partial y}$, $-u\frac{\partial C_{O_2}}{\partial x}$, $-v\frac{\partial C_{O_2}}{\partial y}$) and production and respiration of DO (P) were calculated for the cross-channel wind events and only the time rate of changes of salinity and DO ($\frac{\partial S}{\partial t}, \frac{\partial C_{O_2}}{\partial t}$) and production and respiration of DO (P) were calculated for the along-channel wind events.

3.2.1 Cross-estuary wind events

Cross-channel wind on both June 20th and Sept. 19th drove strong lateral circulation and the halocline was tilted, increasing the lateral gradient of salinity. Lateral advection of salinity dominated over longitudinal advection and controlled the total rate of change of salinity (Figure 6a and 6c). Lateral advection was positive (acted to increase salinity) in the surface layer and negative (acted to decrease salinity) in the bottom layer, decreasing the vertical gradient of salinity. The positive peak in the lateral advection term at about 5 m depth in Figure 6a was due to the oscillations of the halocline, creating an opposite gradient of salinity at that depth and time. A negative cross-channel gradient of salinity at about 5 m depth can be seen in the shipboard transects around station 6, where the AVP was located (Figure 5). Although the basic patterns in the advection ($-v\frac{dS}{dy}$) and rate of change of salinity ($\frac{dS}{dt}$) terms in Figure 6a and 6c were similar, they were not identical, meaning that lateral advection only caused part of the total change of salinity. This imbalance of terms in the salinity budget suggests vertical mixing also played an important role during cross-channel wind events. The role of vertical mixing is investigated further with idealized model simulations in section 4.3.

For the dissolved oxygen (DO) budget (Figure 6b and 6d), lateral advection ($-v\frac{dC_{O_2}}{dy}$) and production and respiration (P) together controlled the total time rate of change of DO ($\frac{dC_{O_2}}{dt}$). Because they were not measured, constant chlorophyll concentration and respiration rate were used to calculate P. The uncertainty in P is therefore large, but the patterns are still informative. The lateral advection terms were negative (reduced DO) in the surface layer and positive (increased DO) in the bottom layer, and thus tended to decrease the vertical oxygen gradient. Near the surface, P was positive and much larger than the advection terms, indicating that photosynthesis dominated changes in DO concentration in the upper water column. P decreased with depth and was negative in the lower water column, meaning respiration dominated over photosynthesis and the term was a sink of DO in the bottom layer. However, the bottom DO was still increasing with time (positive $\frac{dC_{O_2}}{dt}$), due to the larger positive lateral advection term. This reveals that during cross-channel wind events, lateral circulation transports surface higher DO water to the bottom layer and this dominates over respiration.

3.2.2 Down-estuary wind event

During the down-estuary wind event, the wind stress increased with time (Figure 7a), and three different stages can be seen in both $\frac{dS}{dt}$ and $\frac{dC_{O_2}}{dt}$ profiles (Figure 7b and 7c). During the first stage (15:00-17:30, Figure 8a and 8b), $\frac{dS}{dt}$ was close to zero at the surface and increased rapidly from about 5 m depth to the bottom and $\frac{dC_{O_2}}{dt}$ was positive at the surface and decreased rapidly from 5 m depth to the bottom. In this stage, the exchange flow was increased (Figure 8a) and high salinity water was transported up-estuary to the AVP station near the bottom, increasing the density difference between the lower and upper water column and forming two distinct layers. DO was also decreased in the bottom layer due to the increased stratification and associated reduced mixing. In the second stage (17:30-19:30, Figure 8c and 8d), $\frac{dS}{dt}$ was negative in the surface layer and positive in the bottom layer, and the boundary between the two layers was at about 5 m depth. This indicates the along-channel advection was still strong, with the exchange flow transporting fresher water downstream at the surface and saltier water upstream at the bottom. The two layers are also clear from the $\frac{dC_{O_2}}{dt}$ profiles, with the boundary between the two layers at about 5 m depth. Within each layer, $\frac{dC_{O_2}}{dt}$ was negative at the surface and positive at the bottom of each layer, meaning that the DO concentration was not uniform within each layer and there was vertical mixing within each layer but little exchange between the layers. In the final stage (19:30-midnight, Figure 8e and 8f), $\frac{dS}{dt}$ was positive at the surface and negative at the bottom and $\frac{dC_{O_2}}{dt}$ was negative at the surface and positive at the bottom. This indicates that vertical mixing dominated the salinity and DO budgets, and bottom higher salinity and lower DO water was mixed into the upper water column, tending to decrease the stratification.

In these three stages, wind transitioned from acting to increase the exchange flow and strain the along-channel salinity gradient, to acting to mix the whole water column. This transition is evident from the change of the surface mixed layer, the layer near the surface where momentum and dissolved materials are vertically uniform due to wind mixing. The exchange flow increased over time with the increase of the wind speed, and the surface outflow layer (h_s) created by the wind deepened (Figure 7d and 7e). The depth of the most positive $\frac{dC_{O_2}}{dt}$ ($\frac{dC_{O_2}}{dt}_{max}$) near the surface increased with time and matched h_s, indicating $\frac{dC_{O_2}}{dt}_{max}$ was caused by the turbulent mixing at the base of the surface mixed layer. Thus, $\frac{dC_{O_2}}{dt}_{max}$ is used to indicate the depth of the surface mixed layer. The buoyancy frequency (N, where $N^2 = -\frac{g}{\rho}\frac{d\rho}{dz}$) was calculated as an indicator of stratification. The depth of the highest N^2 (N^2_{max}) was used to represent the depth of the layer of strong stratification separating the upper and lower salinity layers. The depth of N^2_{max} decreased at first from 16:00 to 20:00, indicating the bottom layer thickened due to the increase of the exchange flow. h_s and $\frac{dC_{O_2}}{dt}_{max}$ deepened and met the stratification layer at 20:00, producing high vertical mixing at the stratification layer. From here the vertical mixing created by the wind eroded the stratification layer. The depth of N^2_{max} then increased from 20:00 to the end and the stratification weakened.

3.2.3 Up-estuary wind event

During the up-estuary wind on Sept.19th, reversed exchange flow was created initially which increased the salinity at the surface and decreased it at the bottom. The reversed exchange flow disappeared after the water column became vertically uniform (Figure 4b and 9d). The reversed exchange flow decreased the stratification, which made the water column more susceptible to vertical mixing. As the wind stress increased, $\frac{dS}{dt}$ became more positive at the surface (salinity increasing) and more negative at the bottom (salinity decreasing) at first and then reduced to zero in the end (Figure 9b, 10a and 10c). Advection associated with the reverse exchange flow and high vertical mixing together reduced the vertical salinity gradient until the salinity became vertically uniform. Similarly, at first $\frac{dC_{O_2}}{dt}$ became more negative at the surface and more positive at the bottom, then it reduced to zero in the end (Figure 9c, 10b and 10d). This indicates that high vertical mixing transported the surface high DO water to the bottom, mixing up the DO profile.

3.3 Salinity and DO budgets from Idealized Simulations

As it was not possible to calculate every term in the salinity and DO budgets from the field observations, idealized simulations using GOTM were used to further evaluate the role of each term during different types of wind events. Simulations were performed with cross-estuary and up-estuary wind of 5 m/s and downstream winds of 5 m/s, 10 m/s and 15 m/s. The simulations were run for 60 hours (started from midnight) for each wind condition but were run for 1 month for the 10 m/s down-estuary wind condition because it was close to a transition point between wind straining and wind mixing thus it took much longer time to reach steady state. The complete salinity and DO budgets were calculated based on the model output early in the simulation (after 12 hours) and in the end.

Vertical profiles of the eddy diffusivity (K_z) at 12 h and 60 h for four of the five wind condition are shown in Figure 11. For the cross-channel wind, initially K_z was high within the surface layer but decreased rapidly below 4 m above bottom, where the salinity started to increase. After 60 hours, the water column was well mixed (one layer) so K_z was small at the surface and bottom and large in the middle of the water column (Figure 11a). For the up-estuary wind, similar to the cross-channel wind, after 12 h K_z was small within the layer of high stratification between 4 m and 6 m above bottom. After 60 hrs the salinity was uniform throughout and K_z was low at the surface and bottom and high in the middle of the water column (Figure 11b). For the 5 m/s down-estuary wind, stratification increased throughout the 60-hr simulation. There were two well-defined layers and the salinity was uniform within each layer. K_z was high in the middle of each layer and low at the top and bottom of each layer (Figure 11c). For the 15 m/s down-estuary wind, the stratification layer deepened more rapidly compared to the 5 m/s wind situation thus the low K_z layer was deeper than the 5 m/s situation. After 60 hours the water column was well-mixed and K_z was maximum in the middle of the water column, like the cross-channel and up-estuary wind situations (Figure 11d).

3.3.1 Cross-estuary wind

For the cross-channel wind simulations, lateral advection dominated over longitudinal advection due to the strong lateral circulation forced by the wind and the assumed lateral salinity gradient. For the 5 m/s wind, consistent with the observations, high salinity water was initially advected across the estuary in the wind direction in the upper water column and low salinity water was advected in the opposite direction in the lower water column, increasing salinity at the surface and decreasing salinity at the bottom (Figure 12a). The vertical mixing term was largest in the lower water column and it was comparable in size with the lateral advection. Lateral advection and vertical mixing together decreased the salinity at the bottom and increased it at the surface. After 60 hours (Figure 12c), the salinity profile was well mixed and $\frac{dS}{dt}$ was constant throughout the water column and negative due to the downstream depth-averaged current, which caused loss of salt. Lateral advection was balanced by vertical mixing. Similar to the observations, vertical mixing of dissolved oxygen was strong enough to diffuse surface DO produced by photosynthesis to the bottom layer and increase bottom DO (Figure 12b). After 60 hours, the water became well-mixed and the vertical mixing balanced the photosynthesis and respiration (Figure 12d).

3.3.2 Down-estuary wind

Three different down-estuary wind speeds (5, 10, 15 m/s) were simulated and the salinity and DO budgets were calculated for each scenario. For the 5 m/s down-estuary wind, the salinity profile became more stratified with time and the halocline strengthened and deepened initially and finally ceased deepening at 5 m depth (Figure 13a). Salinity increased at the bottom and decreased at the surface due to the along-channel advection (Figure 14a and 14c). Vertical mixing was strong in the stratified layer initially when the halocline was forming, and it balanced along-channel advection in the surface layer but was weak in the strongly stratified layer and in the bottom layer where the salinity gradient was small (Figure 14a). After the halocline ceased deepening, the vertical mixing was strong only in the surface layer where it balanced the along-channel advection and vertical mixing was weak at the halocline and bottom layer (Figure 14c). The cross-channel salinity gradient was set to zero during along-channel wind events thus the lateral advection was zero.

Consistent with the salinity, the vertical DO gradient became stronger with time after the onset of downstream wind and the bottom layer DO ultimately decreased to zero (anoxic, Figure 13b). Vertical mixing was strong in the surface layer and top of the bottom low DO layer when it was still forming and was weak in the layer of strong stratification that separated the upper and lower layers. DO decreased in the bottom layer due to respiration and vertical mixing combined by the sediment oxygen demand. (Figure 14b). After 60 hours when the bottom layer was well-formed and anoxic, the vertical mixing became weak in the stratified layer and bottom layer (Figure 14d). In the surface layer, the vertical mixing brought the DO produced by the photosynthesis to the lower part of the surface layer which was below the euphotic zone.

For the 10 m/s down-estuary wind, similar to the 5 m/s wind situation, the salinity difference between upper and lower layers increased with time and the depth of halocline increased and finally ceased deepening at 5.8 m depth, which was deeper than the 5 m/s situation (Figure 13c). Consistent with the 5 m/s wind situation, the salinity decreased at the surface and increased at the bottom due to along-channel advection, creating a strong halocline. Vertical mixing was strong initially in the stratified layer when the halocline was still deepening. In the end, vertical mixing was strong in the surface layer where it balanced the along-channel advection and dropped at the stratification layer and bottom layer (Figure 15a).

The DO profile followed a similar pattern, with decreasing thickness of the bottom low DO layer over time (Figure 13d). Vertical mixing was strong in the surface layer and top of the bottom low DO layer when it was still forming and was weak in the stratified layer. The bottom DO was not completely depleted, in contrast to the 5 m/s wind situation. In the end, the vertical mixing was strong enough in the surface layer to bring the DO produced by the photosynthesis to the lower part of the surface layer. Mixing was weak at the stratification layer and within the bottom layer (Figure 15b).

When the wind was 15 m/s toward down-estuary, the bottom high salinity layer became thinner more rapidly and went away at about 40 hours, when the salinity profile became well-mixed (Figure 13e). After the water was well-mixed, the vertical mixing diffused bottom high salinity water to the upper water column and along-channel advection transported salt out of this location, causing a net loss of the salt (Figure 15c). The bottom low DO layer also became thinner with time (Figure 13f) and after salinity stratification went away, the vertical mixing became strong and the low DO water was rapidly diffused toward the surface. The DO reached a steady state in which P was balanced by the vertical mixing (Figure 15d).

In conclusion, during the down-estuary wind, the wind initially acted to increase the exchange flow, strain the salinity field, and enhance stratification and hypoxia. For small wind speeds, a steady state was reached in which the surface mixed layer stopped deepening. For larger wind speeds, the surface layer deepened and the bottom layer became thinner. After some time, the effects of wind mixing exceeded the wind straining and the whole water column became well mixed.

3.3.3 Up-estuary wind

For the up-estuary wind, the wind always acted primarily to mix the water column, decreasing the stratification and generating vertical mixing. The halocline deepened and finally disappeared (Figure 13g). Salinity initially decreased at the bottom and increased at the surface due to along-channel advection. Vertical mixing happened within each layer and was strong at the stratified layer separating the upper and lower layers, acting to erode the stratification (Figure 16a). After 60 hours (Figure 16c), the salinity profile became uniform and along-channel advection due to the reversed exchange flow was balanced by convective vertical mixing throughout the water column. The bottom low DO layer became thinner as well over time and after the water column was well-mixed, the bottom low DO water was quickly mixed upward (Figure 13h). DO increased at the stratification layer separating the upper and lower layers due to the high vertical mixing (Figure 16b). The bottom layer DO continued to decrease due to vertical mixing combined with sediment oxygen demand when the stratification still existed. Along-channel advection was weak compared to vertical mixing because of the weak along-channel gradient of DO. After 60 hours when the salinity was well-mixed, the DO reached a steady state in which the vertical mixing balanced the P (Figure 16d).

4 Discussion

4.1 Influence of wind direction and speed on salinity and oxygen dynamics

Lateral circulation can be driven under different wind cases and modulates the salinity and DO profile simultaneously. In this study, we observed lateral circulation that was driven by cross-estuary winds that acted to tilt isopycnals, and thus reduce vertical stratification and increase bottom DO. This differs from previous work in the Chesapeake Bay that reported lateral circulation driven by along-channel winds. Li and Li (2012) showed, from model simulations in the Chesapeake Bay, along-channel winds drive strong lateral circulations due to the Ekman transport caused by Coriolis effect. Isopycnals are tilted in the across-channel direction, which creates high lateral baroclinic pressure gradient and interacts back with the Ekman transport. In the NRE, the average water depth (< 4 m) is much less than the Ekman layer thickness [*Csanady*, 1967]. Thus, the lateral circulations observed in this study are primarily driven by the cross-channel winds. Reynolds-Fleming and Luettich (2004) measured salinity and DO profiles at each side of the upper NRE and found a correspondence between high salinity and low DO in the bottom water on each side of the estuary under cross-channel winds. The present study provides a more complete view of salinity and DO cross-sections and cross-estuary circulation under different wind conditions. The bottom high salinity and low DO layer is clearly shown to be pushed to the side of the estuary due to lateral circulation under cross-channel winds. Furthermore, salinity and DO budgets show that lateral circulations cause high lateral advection that decreases the vertical gradients of salinity. This promotes vertical mixing, which combines with the lateral advection to make the salinity and DO profiles vertically uniform.

Along-channel winds not only serve as an energy source for turbulence mixing but can also alter the exchange flow and strain the along-channel salinity gradient to modify vertical stratification. Scully et al. (2005) found that in the York River Estuary in Virginia, down-estuary winds enhance the exchange flow, strain the along-channel density field and increase the stratification while up-estuary winds reduce them. In this study, reversed exchange flow was observed during up-estuary winds, causing advection that decreased the stratification ultimately leading to high vertical mixing. Chen and Sanford (2009) simulated an idealized estuary and found that the exchange flow and stratification first increase then decrease as down-estuary wind speed increases. In this study, both the observations and model results capture the deepening of the surface mixed layer after the onset of down-estuary wind. From observations, as the wind increased, the exchange flow and stratification increased at first and then decreased and finally disappeared after the surface mixed layer reached the stratification layer and created strong vertical mixing.

The simulations further reveal that under small and moderate speeds (5 and 10 m/s), wind acts primarily to strain the along-estuary salinity gradient even though the bottom high salinity layer becomes thinner with the increase of the wind speed. Only after the wind exceeds a threshold (15 m/s) does vertical mixing dominate over straining and erode the stratification layer until it disappears. Chen and Sanford (2009) derived a modified horizontal Richardson number ($Ri_{x,new}$), a ratio of vertical buoyancy flux due to turbulent diffusion (B_{turb}) to horizontal buoyance flux (B_{shear}), to include wind straining and wind mixing. The wind straining prevails when $Ri_{x,new} > 1$ and vice versa. For our study, we calculated $Ri_{x,new}$ based on model output once steady state was reached. The results are consistent with former findings. $Ri_{x,new}$ is 4.56 during 5 m/s wind and 1.05 during 10 m/s wind, meaning the wind straining dominates. $Ri_{x,new}$ reduces to 0.48 (< 1) during 15 m/s wind, meaning the wind mixing prevails.

DO dynamics follow the changes in estuarine circulation and stratification and are also influenced by biological processes. Scully (2010b) simulated the changes of the volume of bottom hypoxic water under different wind conditions in the Chesapeake Bay. Their goal was to isolate the role of physical processes on oxygen dynamics by assuming the biological processes are constant in both time and space. They assume the respiration rate is a constant throughout the estuary and no photosynthesis. They include the air-sea exchange but neglect the sediment oxygen demand. Compared to a no wind situation, they found that winds coming from all directions

(N,S,E,W) tend to decrease the bottom hypoxia volume, although the extent differs. Lateral circulation due to Ekman transport and vertical mixing caused by the decrease of stratification are two dominant reasons. In this study, more complete biological processes are considered as the photosynthesis and sediment oxygen demand are taken into account. Photosynthesis in the surface layer tends to increase the vertical gradient of the DO, which could contribute to a higher vertical turbulent diffusive DO flux through the halocline, increasing the bottom layer DO concentration. Sediment oxygen demand acts as a sink at the bottom boundary and tends to create a vertical gradient of DO close to the seabed, inducing vertical mixing to diffuse DO from the water to the seabed and decreasing bottom layer DO. Thus the competition of these two effects, accompanied with the physical processes, controls the overall value of the vertical mixing within the bottom layer. When the stratification is strong (5 and 10 m/s down-estuary wind scenarios), the turbulent flux of DO through the halocline is weaker than bottom layer respiration and the sediment oxygen demand reducing the bottom layer DO concentration. When the stratification is eroded (observations, 15 m/s down-estuary wind and up-estuary wind scenarios), vertical mixing of DO through the halocline is stronger than the combined sediment oxygen demand and bottom layer respiration, increasing the bottom layer DO. Lateral advection caused by lateral circulation is strong under cross-channel winds and combines with vertical mixing to increase the bottom DO.

4.2 Response of stratification and bottom DO to wind over 6-month deployment

While the general pattern that the ΔS increased during down-estuary wind and decreased during up-estuary wind and the bottom DO is inversely corelated with it holds over the 6-month period, there are several interesting exceptions. One exception is the event between June 15th to 16th (second black box in Figure 2). The wind blew toward downstream and the bottom DO decreased at first but quickly increased again even though the stratification kept increasing. Because the patterns in salinity and DO are different, this decrease in DO is clearly the result of advection rather than vertical mixing. This might result from a change in the horizontal gradient of the DO, meaning the exchange flow brought higher DO water to the bottom of the study area through along-channel advection. Another exception is the event from June 20th to 21st that was analyzed and discussed above (third black box in Figure 2). During this event, the downstream wind strength and duration were sufficient that the surface mixed layer continued to thicken and wind mixing ultimately eroded the stratification completely causing the water column to become well-mixed.

The cross-channel wind component was usually less important than the along-channel wind component for the stratification and DO dynamics as the ΔS and bottom DO are better correlated to along-channel component than cross-channel component in this 6-month period. But the effect of the lateral circulation to increase bottom DO could become dominant when the along-channel component was weak or the cross-channel component was strong. A typical example is the event between June 11th and 12th (first black box in Figure 2). The wind switched from upstream to downstream but at the same time the cross-channel part of the wind increased rapidly and became sufficiently strong that the homogenizing effect of the cross-channel wind component dominated over the straining effect of the downstream wind component, so stratification decreased and bottom DO increased. Another example of dynamics driven by the cross-channel wind component is the event between June 24th to 28th when the cross-channel wind component switched from positive to negative, ΔS increased and then decreased, and the bottom DO decreased and then increased. The bottom high salinity and low DO layer was presumably pushed from one side of the estuary to the other side. The isopycnals and oxyclines flattened at first to increase the stratification and decrease the bottom DO locally and then tilted again in the opposite direction to decrease the stratification and increase the bottom DO.

The response of the salinity and DO distributions to wind events in the Neuse are complex but follow some general patterns. The bottom high salinity region generally corresponds with the bottom low DO region. Stratification increases and bottom DO decreases only under small and moderate down-estuary wind situations. For all the other directions and speeds, wind tends to decrease the stratification and increase bottom DO, although the mechanisms differ depending on wind direction. When the wind is not purely along- or cross-channel, the interaction of these two parts together determines the hydrodynamics and DO dynamics in the estuary, and this is a topic that requires further study.

5 Conclusions

In this study, based on the observations and calculations of salinity and DO budgets from field data and GOTM simulations, we found distinct effects of the wind on salinity and DO distributions, depending on its direction and speed. Cross-channel wind drives lateral circulation and tilts isohalines and oxyclines, decreasing stratification, enhancing mixing and increasing bottom DO. Down-estuary wind can increase or decrease exchange flow and stratification, depending on the wind speed and duration. After the onset of down-estuary wind, exchange flow increases first, strengthening stratification and decreasing bottom DO. Wind also generates a surface boundary layer with high vertical mixing that deepens over time. Surface mixed layer deepening is halted by stratification at some depth, which increases with wind speed. For faster wind speeds, the layer of strong stratification can be eroded and bottom DO increases. Up-estuary wind decreases and can even reverse the exchange flow, decreasing stratification, and promoting vertical mixing that homogenizes the salinity and DO profiles.

Our 6-month dataset illustrates that, while the patterns described above generally hold for purely across- or along-channel wind events, wind effects on estuarine dynamics and hypoxia are considerably more complex than this idealized picture because the wind direction can be at any angle to the estuarine axis and it varies continuously with time. Additionally, the biological processes of photosynthesis, respiration and sediment oxygen demand are known to vary in space and time, and significantly affect the DO budget and distribution. While this study illustrates that wind can profoundly affect salinity and DO distributions in estuaries both directly, though wind mixing and advection by wind-driven along-estuary and lateral circulation, and indirectly through straining of the density field which modifies stratification and hence vertical mixing, further work on the complexities is clearly needed.

Acknowledgements

We gratefully acknowledge Ryan Neve and David Marshall for help with all aspects of the field measurements, as well as the many people who assisted with the shipboard measurements. Funding for this research came from the NCDEQ Coastal Recreational Fishing License Grants program. Data from the ModMon dataset (https://paerllab.web.unc.edu/modmon/) were also used in this study.

Open Research:

Observation datasets and model input files are available online (https://doi.org/10.5061/dryad.7sqv9s4zh).

References:

Altieri, A. H., and K. B. Gedan (2015), Climate change and dead zones, *Global Change Biology*, *21*(4), 1395-1406, doi:10.1111/gcb.12754.

Blanton, J. O., J. A. Amft, D. K. Lee, and A. Riordan (1989), Wind stress and heat fluxes observed during winter and spring 1986, *Journal of Geophysical Research*, *94*(C8), doi:10.1029/JC094iC08p10686.

Breitburg, D., et al. (2018), Declining oxygen in the global ocean and coastal waters, *Science*, *359*(6371), doi:10.1126/science.aam7240.

Buzzelli, C. P., R. A. Luettich Jr, H. W. Paerl, J. Fear, J. Fleming, L. Twomey, B. Peierls, E. Clesceri, M. J. Alperin, and C. S. Martens (2002a), Neuse River Estuary Modeling and Monitoring Project Phase 2: Monitoring of Hydrography and Water Quality, Circulation, Phytoplankton Physiology and Sediment-Water Coupling, *Water Resources Research Institute of the University of North Carolina, Raleigh, NC*.

Buzzelli, C. P., R. A. Luettich Jr, S. P. Powers, C. H. Peterson, J. E. McNinch, J. L. Pinckney, and H. W. Paerl (2002b), Estimating the spatial extent of bottom-water hypoxia and habitat degradation in a shallow estuary, *Marine ecology progress series*, *230*, 103-112.

Christian, R. R., W. L. Bryant, and D. W. Stanley (1986), The relationship between river flow and Microcystis aerunginosa blooms in the Neuse River, North Carolina, *Water Resources Research Institute of the University of North Carolina, Raleigh, NC*, *Report No. 223.*

Csanady, G. T. (1967), On the “resistance law” of a turbulent Ekman layer, *Journal of Atmospheric Sciences*, *24(5)*, 467-471, doi:10.1175/1520-0469(1967)024<0467:OTLOAT>2.0.CO;2.

Cui, Y., J. Wu, J. Ren, and J. Xu (2019), Physical dynamics structures and oxygen budget of summer hypoxia in the Pearl River Estuary, *Limnology and Oceanography*, *64*(1), 131-148, doi:10.1002/lno.11025.

Diaz, R. J. (2001), Overview of hypoxia around the world, *Journal of environmental quality*, *30*(2), 275-281, doi:10.2134/jeq2001.302275x.

Diaz, R. J., and R. Rosenberg (2008), Spreading dead zones and consequences for marine ecosystems, *science*, *321(5891)*, 926-929, doi:10.1126/science.1156401.

Hagy, J. D., W. R. Boynton, C. W. Keefe, and K. V. Wood (2004), Hypoxia in Chesapeake Bay, 1950–2001: long-term change in relation to nutrient loading and river flow, *Estuaries*, *27*, 634-658, doi:10.2307/1353476.

Jassby, A. D., and T. Platt (1976), Mathematical formulation of the relationship between photosynthesis and light for phytoplankton, *Limnology and Oceanography*, *21*(4), 540-547, doi:10.4319/lo.1976.21.4.0540.

Katin, A., D. Del Giudice, and D. R. Obenour (2019). Modeling biophysical controls on hypoxia in a shallow estuary using a Bayesian mechanistic approach. *Environmental Modeling & Software, 120*. 104491.

Kato, H., and O. M. Phillips (2006), On the penetration of a turbulent layer into stratified fluid, *Journal of Fluid Mechanics*, *37*(4), 643-655, doi:10.1017/s0022112069000784.

Keeling, R. F., A. Körtzinger, and N. Gruber (2010), Ocean Deoxygenation in a Warming World, *Annual Review of Marine Science*, *2*(1), 199-229, doi:10.1146/annurev.marine.010908.163855.

Ladwig, R., L. A. Rock, and H. A. Dugan (2021), Impact of salinization on lake stratification and spring mixing, *Limnology and Oceanography Letters*, *8*(1), 93-102, doi:10.1002/lol2.10215.

Lange, X., and H. Burchard (2019), The Relative Importance of Wind Straining and Gravitational Forcing in Driving Exchange Flows in Tidally Energetic Estuaries, *Journal of Physical Oceanography*, *49*(3), 723-736, doi:10.1175/jpo-d-18-0014.1.

Lee, Y. J., and K. M. M. Lwiza (2008), Characteristics of bottom dissolved oxygen in Long Island Sound, New York, *Estuarine, Coastal and Shelf Science*, *76*(2), 187-200, doi:10.1016/j.ecss.2007.07.001.

Li, Y., and M. Li (2012), Wind-driven lateral circulation in a stratified estuary and its effects on the along-channel flow, *Journal of Geophysical Research: Oceans*, *117*(C9), doi:10.1029/2011jc007829.

Luettich Jr, R. A., J. E. McNinch, H. W. Paerl, C. H. Peterson, J. T. Wells, M. J. Alperin, C. S. Martens, and J. L. Pinckney (2000), Neuse River Estuary modeling and monitoring project stage 1: hydrography and circulation, water column nutrients and productivity, sedimentary processes and benthic-pelagic coupling, and benthic ecology, *Water Resources Research Institute of the University of North Carolina*, *325B*.

Mellor, G. L., and T. Yamada (1982), Development of a turbulence closure model for geophysical fluid problems, *Reviews of Geophysics*, *20(4)*, 851-875, doi:10.1029/RG020i004p00851.

Officer, C. B., R. B. Biggs, J. L. Taft, L. E. Cronin, M. A. Tyler, and W. R. Boynton (1984), Chesapeake Bay anoxia: origin, development, and significance, *Science*, *223(4631)*, 22-27, doi:10.1126/science.223.4631.22.

Oviatt, C. A., D. T. Rudnick, A. A. Keller, P. A. Sampou, and G. T. Almquist (1986), A comparison of system (O-2 and CO2) and C-14 measurements of metabolism in estuarine mesocosms, *Marine Ecology Progress Series*, *28*, 57-67, doi:10.3354/meps028057.

Reed, D. C., and J. A. Harrison (2016), Linking nutrient loading and oxygen in the coastal ocean: A new global scale model, *Global Biogeochemical Cycles*, *30*(3), 447-459, doi:10.1002/2015gb005303.

Reynolds-Fleming, J. V., J. G. Fleming, and R. A. Luettich (2002), Portable autonomous vertical profiler for estuarine applications, *Estuaries*, *25*, 142-147, doi:10.1007/BF02696058.

Reynolds-Fleming, J. V., and R. A. Luettich (2004), Wind-driven lateral variability in a partially mixed estuary, *Estuarine, Coastal and Shelf Science*, *60*(3), 395-407, doi:10.1016/j.ecss.2004.02.003.

Riemann, B., et al. (2015), Recovery of Danish Coastal Ecosystems After Reductions in Nutrient Loading: A Holistic Ecosystem Approach, *Estuaries and Coasts*, *39*(1), 82-97, doi:10.1007/s12237-015-9980-0.

Rizzo, W. M., and R. R. Christian (1996), Significance of subtidal sediments to heterotrophically-mediated oxygen and nutrient dynamics in a temperate estuary, *Estuaries*, *19*, 475-487, doi:10.2307/1352464.

Sanford, L. P., and S.-N. Chen (2009), Axial Wind Effects on Stratification and Longitudinal Salt Transport in an Idealized, Partially Mixed Estuary*, *Journal of Physical Oceanography*, *39*(8), 1905-1920, doi:10.1175/2009jpo4016.1.

Schumann, U., and T. Gerz (1995), Turbulent mixing in stably stratified shear flows, *Journal of Applied Meteorology and Climatology*, *34(1)*, 33-48, doi:10.1175/1520-0450-34.1.33.

Scully, M. E. (2010a), The Importance of Climate Variability to Wind-Driven Modulation of Hypoxia in Chesapeake Bay, *Journal of Physical Oceanography*, *40*(6), 1435-1440, doi:10.1175/2010jpo4321.1.

Scully, M. E. (2010b), Wind Modulation of Dissolved Oxygen in Chesapeake Bay, *Estuaries and Coasts*, *33*(5), 1164-1175, doi:10.1007/s12237-010-9319-9.

Scully, M. E. (2013), Physical controls on hypoxia in Chesapeake Bay: A numerical modeling study, *Journal of Geophysical Research: Oceans*, *118*(3), 1239-1256, doi:10.1002/jgrc.20138.

Scully, M. E., C. Friedrichs, and J. Brubaker (2005), Control of estuarine stratification and mixing by wind-induced straining of the estuarine density field, *Estuaries*, *28*, 321-326, doi:10.1007/BF02693915.

Simpson, J. H., and D. Bowers (1981), Models of stratification and frontal movement in shelf seas., *Deep Sea Research Part A. Oceanographic Research Papers*, *28(7)*, 727-738., doi:10.1016/0198-0149(81)90132-1.

Simpson, J. H., J. Sharples, and T. P. Rippeth (1991), A prescriptive model of stratification induced by freshwater runoff, *Estuarine, Coastal and Shelf Science*, *33(1)*, 23-35, doi:10.1016/0272-7714(91)90068-M.

Smith, L. M., C. M. Silver, and C. A. Oviatt (2012), Quantifying variation in water column photosynthetic quotient with changing field conditions in Narragansett Bay, RI, USA, *Journal of Plankton Research*, *34*(5), 437-442, doi:10.1093/plankt/fbs011.

Umlauf, L., H. Burchard, and K. Bolding (2005), GOTM sourcecode and test case documentation, *Devel version-pre, 4.*

Wanninkhof, R., W. E. Asher, D. T. Ho, C. Sweeney, and W. R. McGillis (2009), Advances in quantifying air-sea gas exchange and environmental forcing, *Annual review of marine science*, *1*, 213-244, doi:10.1146/annurev.marine.010908.163742.

Whipple, A. C., R. A. Luettich, and H. E. Seim (2006), Measurements of Reynolds stress in a wind-driven lagoonal estuary, *Ocean Dynamics*, *56*, 169-185, doi:10.1007/s10236-005-0038-x.

Xie, X., and M. Li (2018), Effects of Wind Straining on Estuarine Stratification: A Combined Observational and Modeling Study, *Journal of Geophysical Research: Oceans*, *123*(4), 2363-2380, doi:10.1002/2017jc013470.

Table 1. Values and units of parameters used in Eq. 3 to Eq. 6.

Parameters	Values
PQ	1.24
$C_{chl}\ (mg/L)$	0.03
$P_{max}\ (mg_{carbon}/mg_{chl}/s)$	0.0012
α	0.0518
$K_d(1/m)$	-1.27
$I_{max}\ (\mu mol/m^2/s)$	2000

Table 2. Values and units of parameters for the simulations.

Parameters	Values
Down-estuary wind (m/s)	5; 10; 15
Up-estuary wind (m/s)	5
Cross-channel wind (m/s)	5
$\frac{\partial S}{\partial x}\ (PSU/m)$	1.20×10^{-4}
$\frac{\partial S}{\partial y}\ (PSU/m)$	-1.05×10^{-4}
$\frac{\partial C_{O_2}}{\partial x}\ (mg/(L*s))$	1.68×10^{-5}
$\frac{\partial C_{O_2}}{\partial y}\ (mg/(L*s))$	3.51×10^{-4}
River Inflow (m/s)	0.01
z_0(m)	6.8×10^{-3}
C_d	1.14×10^{-3}

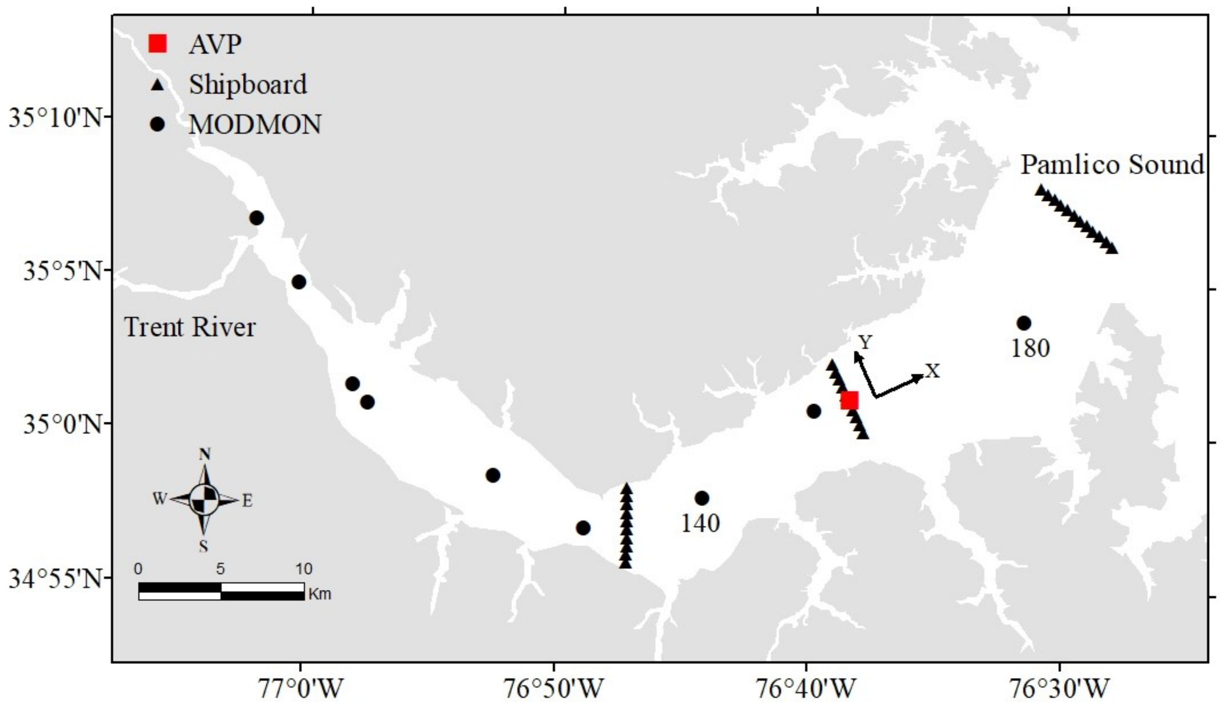

Figure 1. Study area and observation sites in the Neuse Estuary. The red rectangle is the central station where the AVP and ADCP were located. The black triangles indicate shipboard observation sites. The black circles are the MODMON stations, with stations 140 and 180 indicated.

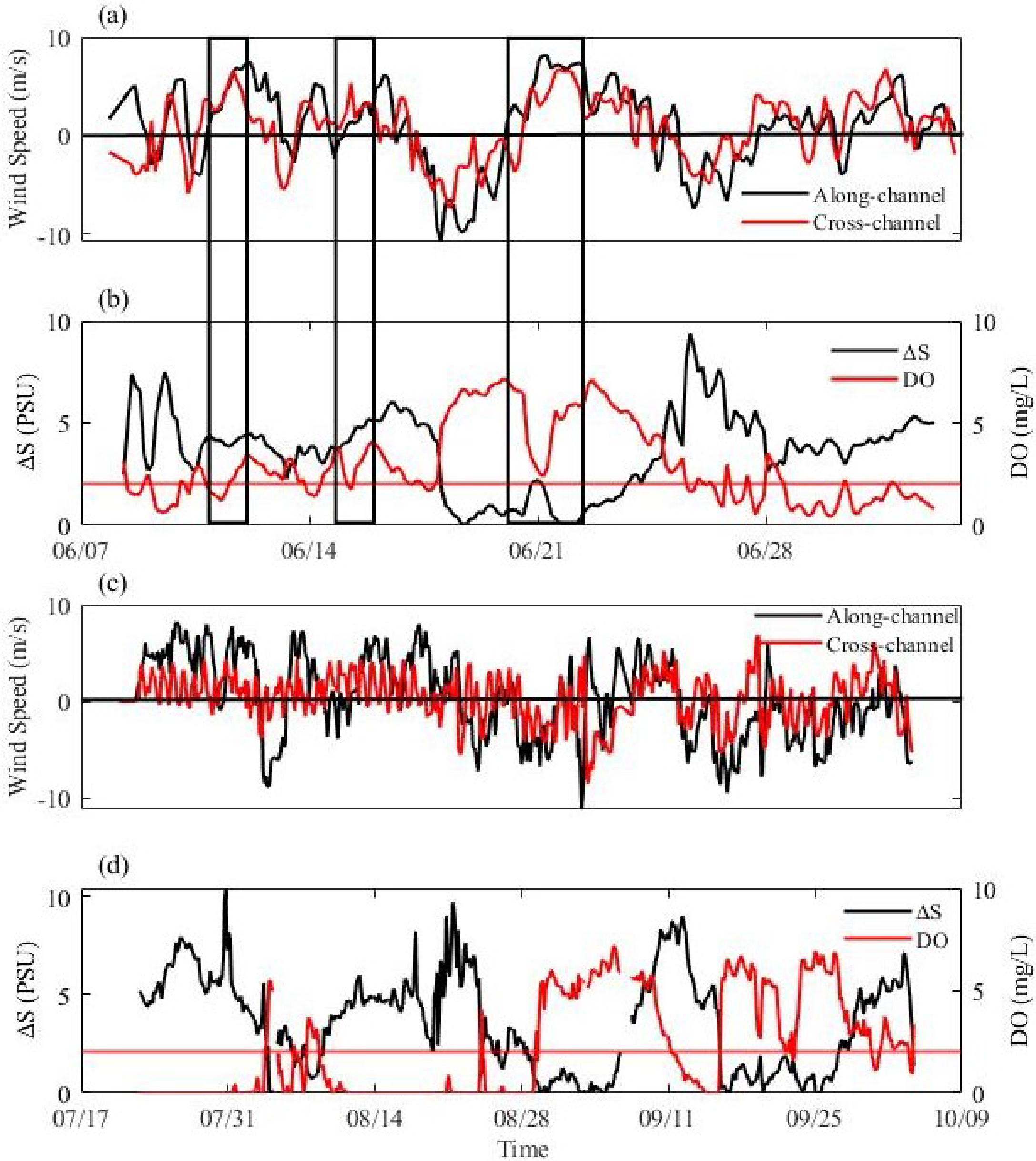

Figure 2. Time series of 3h-averaged along-channel wind (black), cross-channel wind (red), salinity difference between surface and bottom 0.5 m (ΔS, black) and DO averaged over bottom 0.5 m (red) from a,b): June 8th to July 4th and c,d): July 20th to October 4th. In a) and c), the black line is 0 m/s wind. In b) and d), left y-axis is ΔS and right y-axis is DO and the red line is 2 mg/L for DO. Positive value for along-channel wind means towards downstream and for cross-channel wind means toward the north shore.

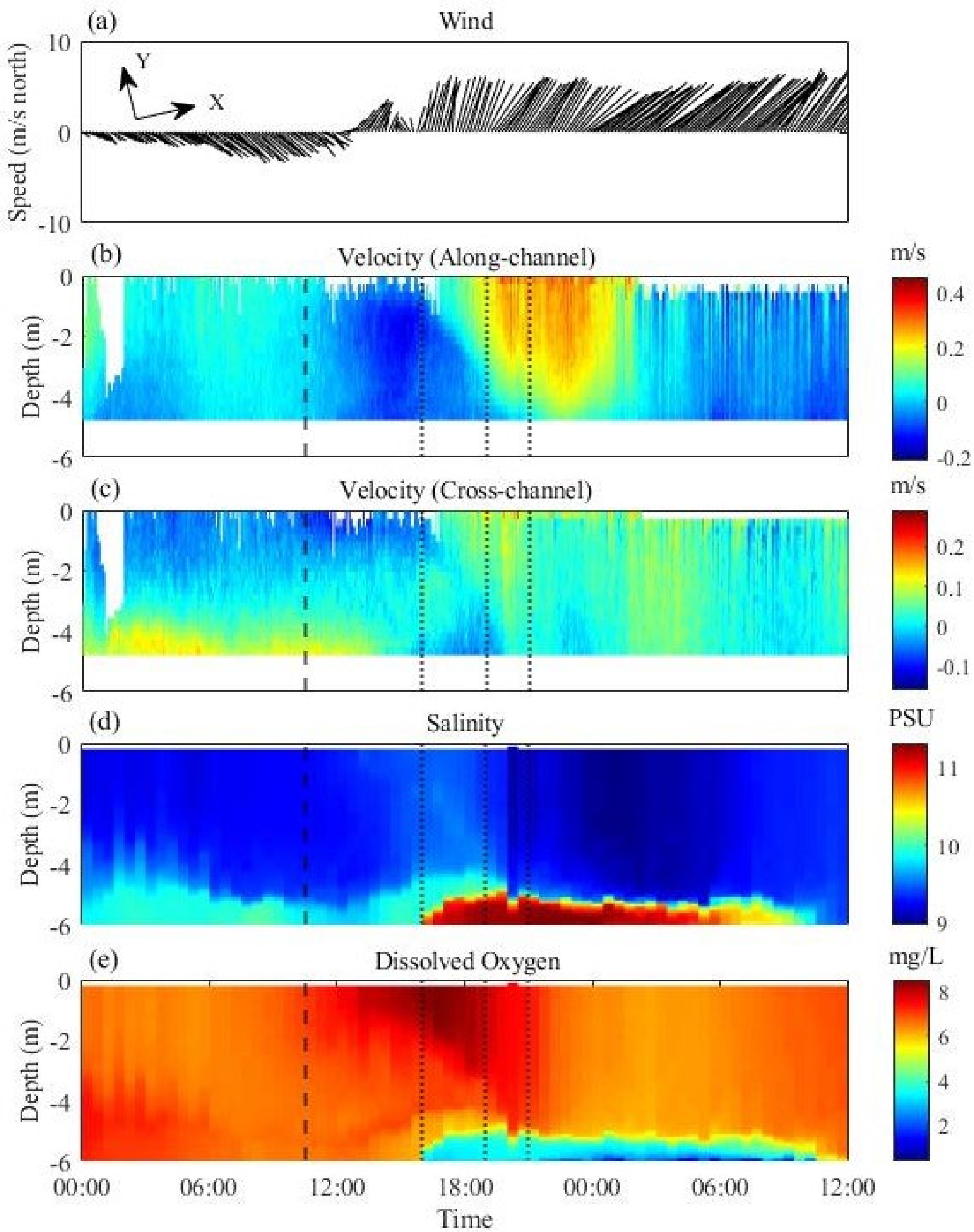

Figure 3. Time series of a) wind velocity, b) along-channel velocity component, c) cross-channel velocity component, d) salinity) and e) dissolved oxygen on June 20th and June 21st at AVP station. Positive along-channel is toward down-estuary and positive cross-channel is toward the north shore. The black dashed line is the time (10:30) for the budget calculations for the cross-channel wind case. The black dotted lines are the times (16:00, 19:00, 21:00) for the budget calculations for the down-estuary wind case.

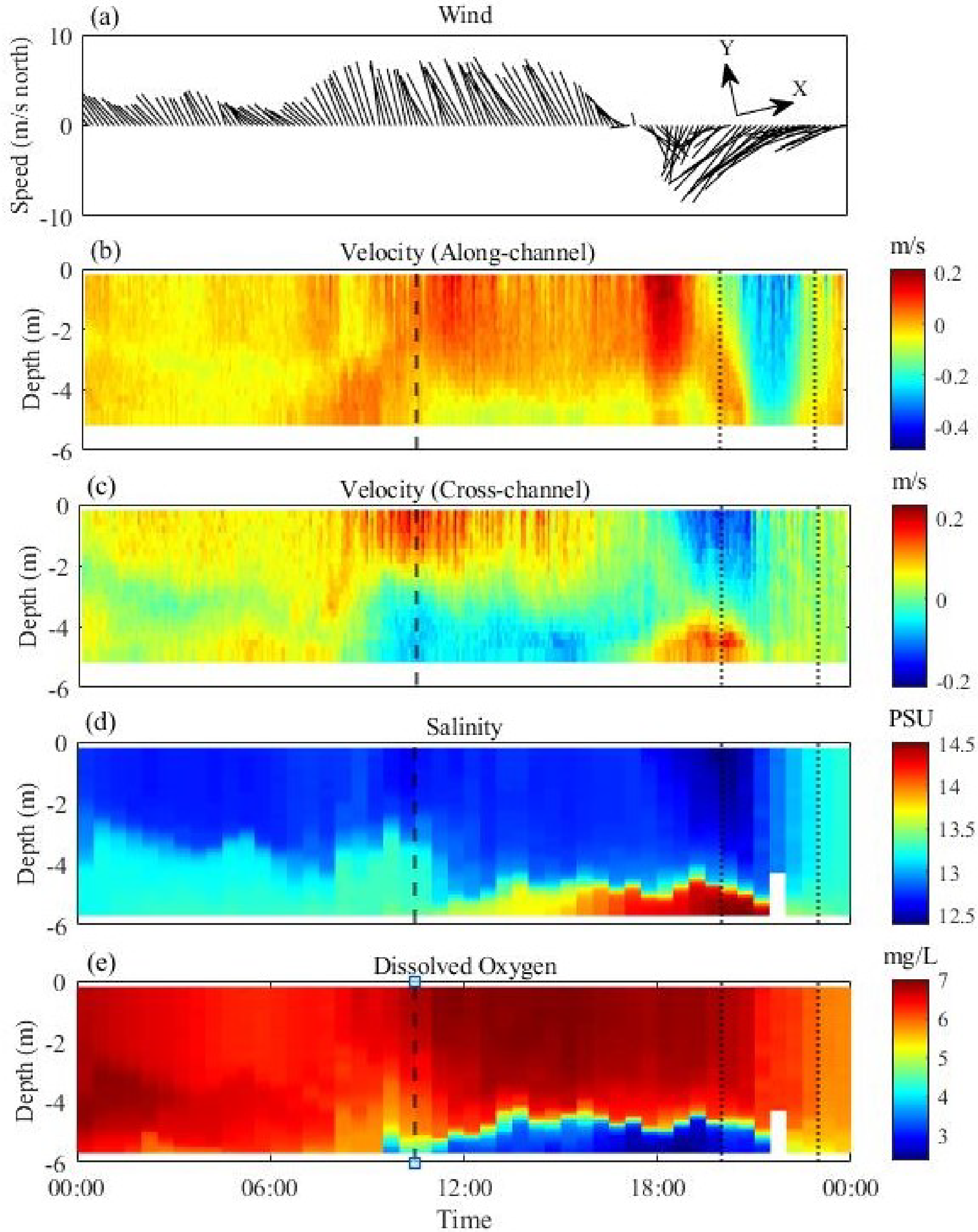

Figure 4. Time series of a) wind velocity, b) along-channel velocity, c) cross-channel velocity, d) salinity, and e) dissolved oxygen on Sept. 19th at the AVP station. Positive along-channel is down-estuary and positive cross-channel is toward the north shore. The black dashed line is the time (10:30) for the budget calculations for the cross-channel wind case. The black dotted lines are the times (20:00, 23:00) for the budget calculations for the up-estuary wind case.

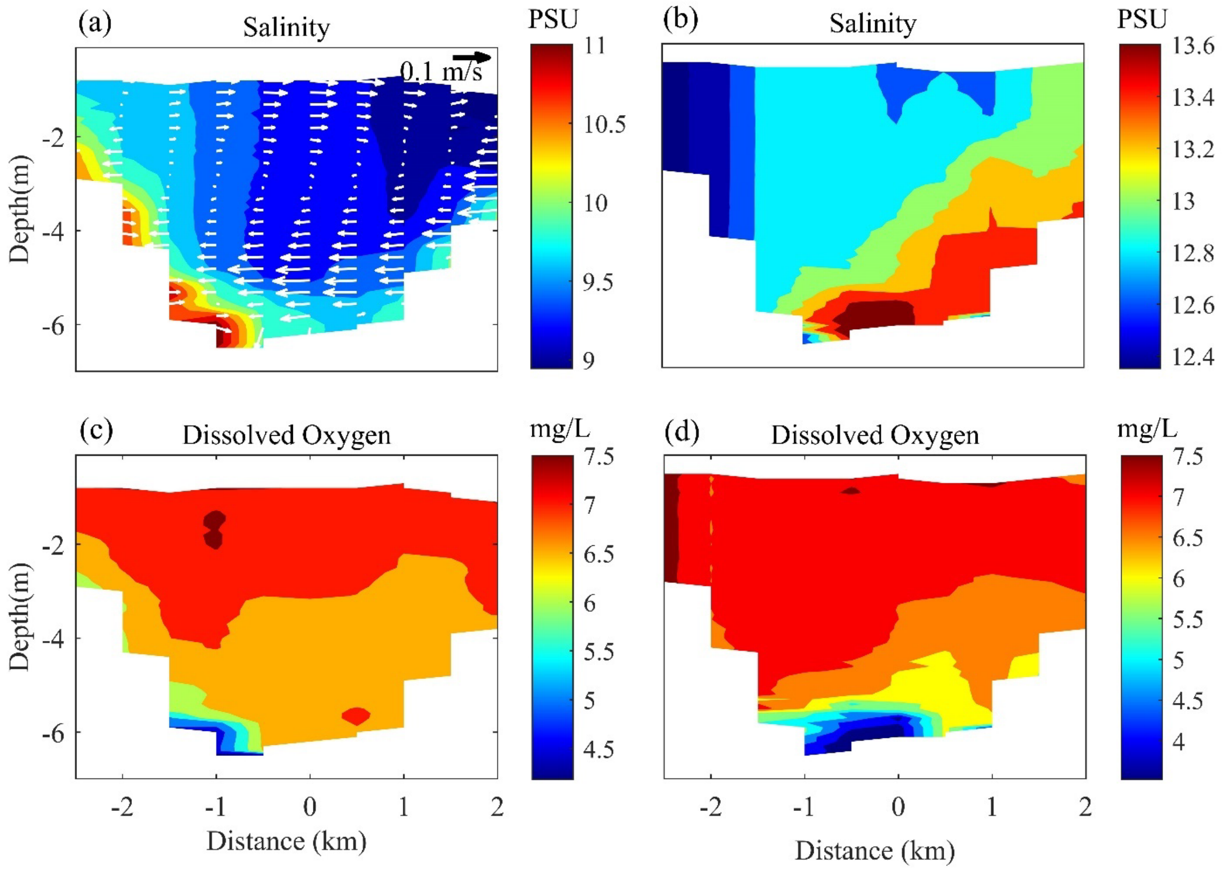

Figure 5. Contours of salinity and dissolved oxygen across the estuary at the central shipboard transect at noon on (a, c) June 20th and (b, d) Sept. 19th. X-axis is the distance to the central (AVP) station. The distance between each station is 500 m. The left side is the north shore and the right side is the south shore and the profiles are looking down-estuary. The white arrows in (a) are the cross-channel velocity.

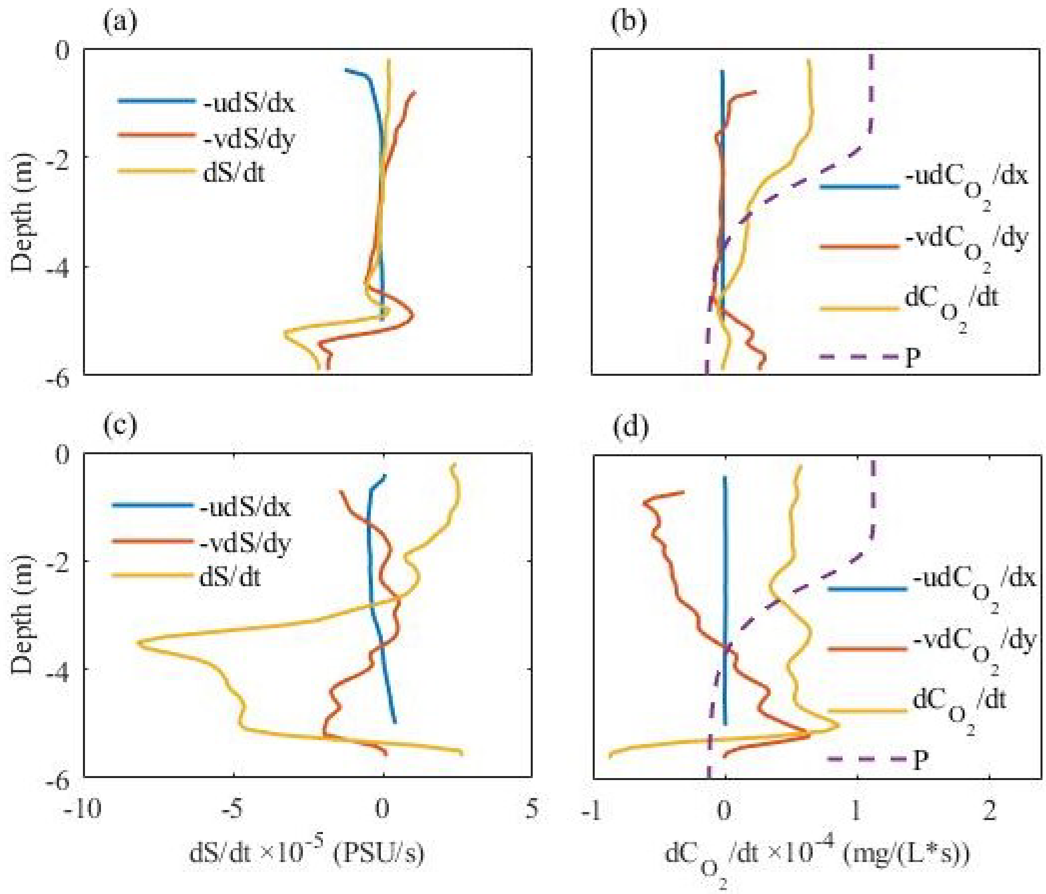

Figure 6. Vertical profiles of salinity and dissolved oxygen budget terms for the cross-channel wind at 10:30 on (a, b) June 20th and (c, d) Sept. 19th. Blue and red curves are the along-channel and cross-channel advection terms and the yellow curve is the total time rate of change of the salinity or dissolved oxygen concentration. The dashed purple curve is the net production term, the sum of production and respiration.

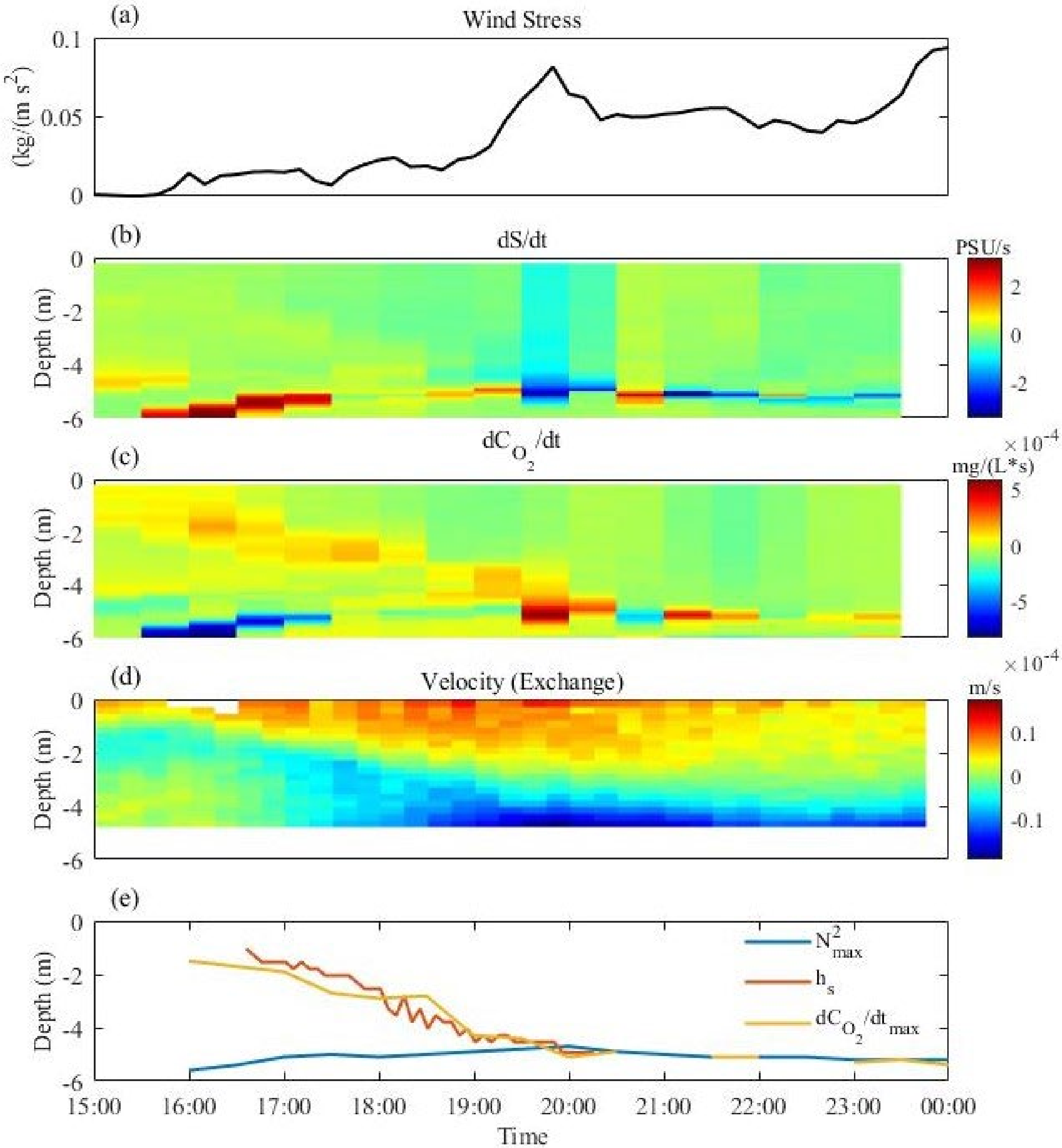

Figure 7. Time series of a) the along channel wind stress, b) the time rate of change of salinity, c) time rate of change of dissolved oxygen, d) exchange velocity (actual minus depth-average velocity) and e) depths of the highest buoyancy frequency (N^2, blue), depths of the surface outflow layer (h_s, red) and the depths of the highest positive $\frac{dC_{O_2}}{dt}$ (yellow) on June 20th during the down-estuary wind event.

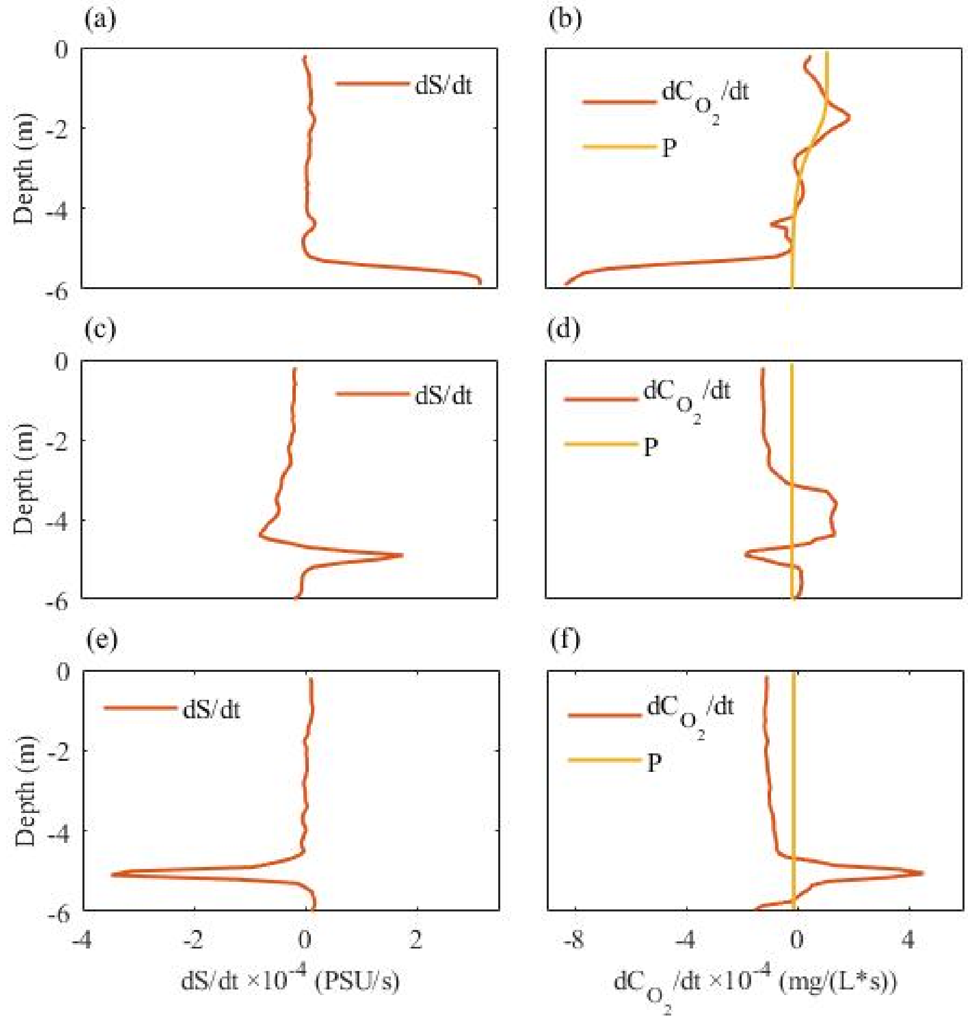

Figure 8. Vertical profiles of the time rate of change of (a,c,e) salinity, and (b,d,f) dissolved oxygen (red) along with production and respiration (yellow) during the down-estuary wind event at (a,b) 16:00, (c,d) 19:00 and (e,f) 21:00 on June 20th.

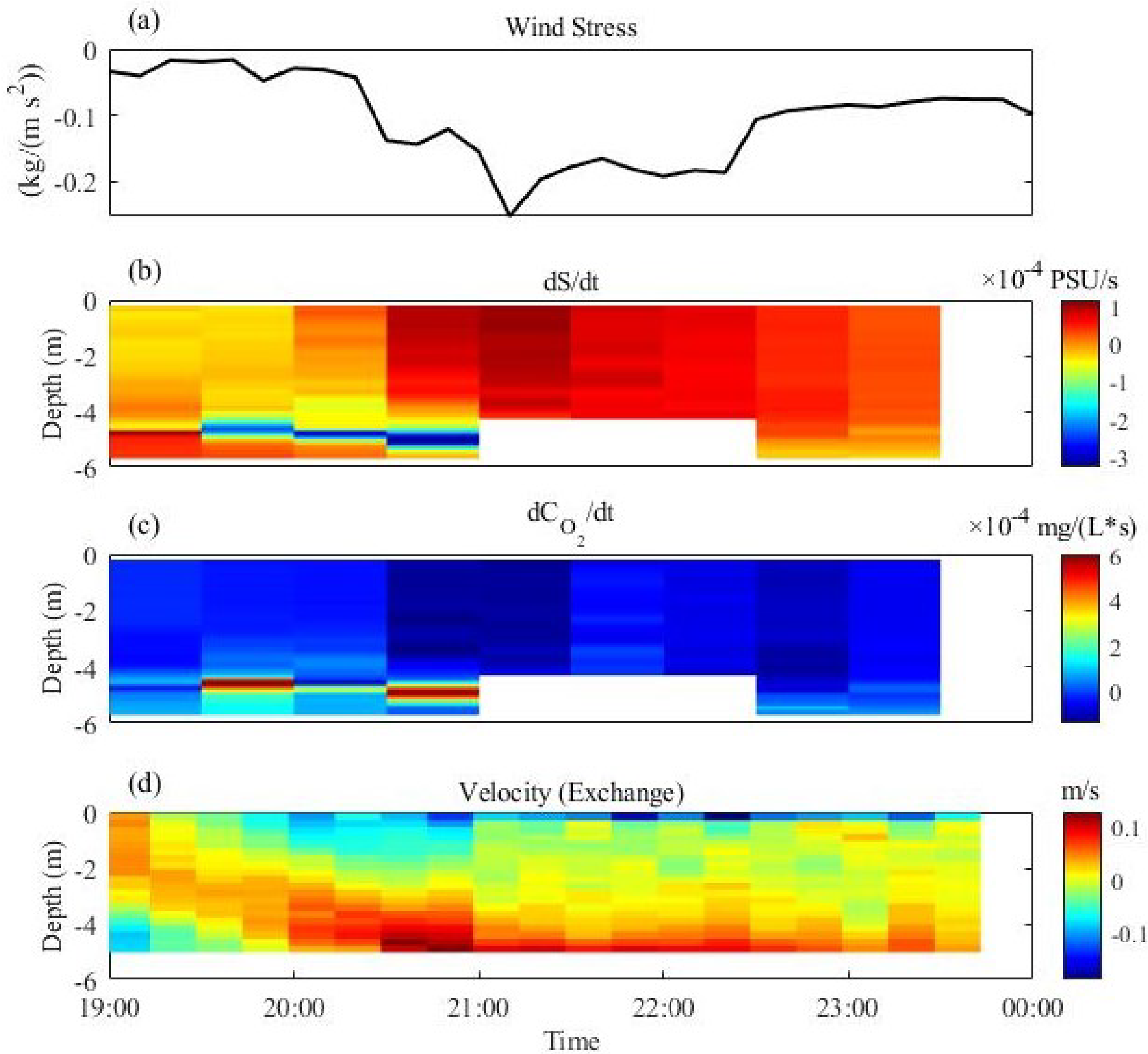

Figure 9. Time series of a) along-channel wind stress, b) the time rate of change of salinity, c) time rate of change of dissolved oxygen and d) exchange velocity (actual velocity minus depth-averaged velocity) during the up-estuary wind event on Sept. 19th from 19:00 to the end of the day.

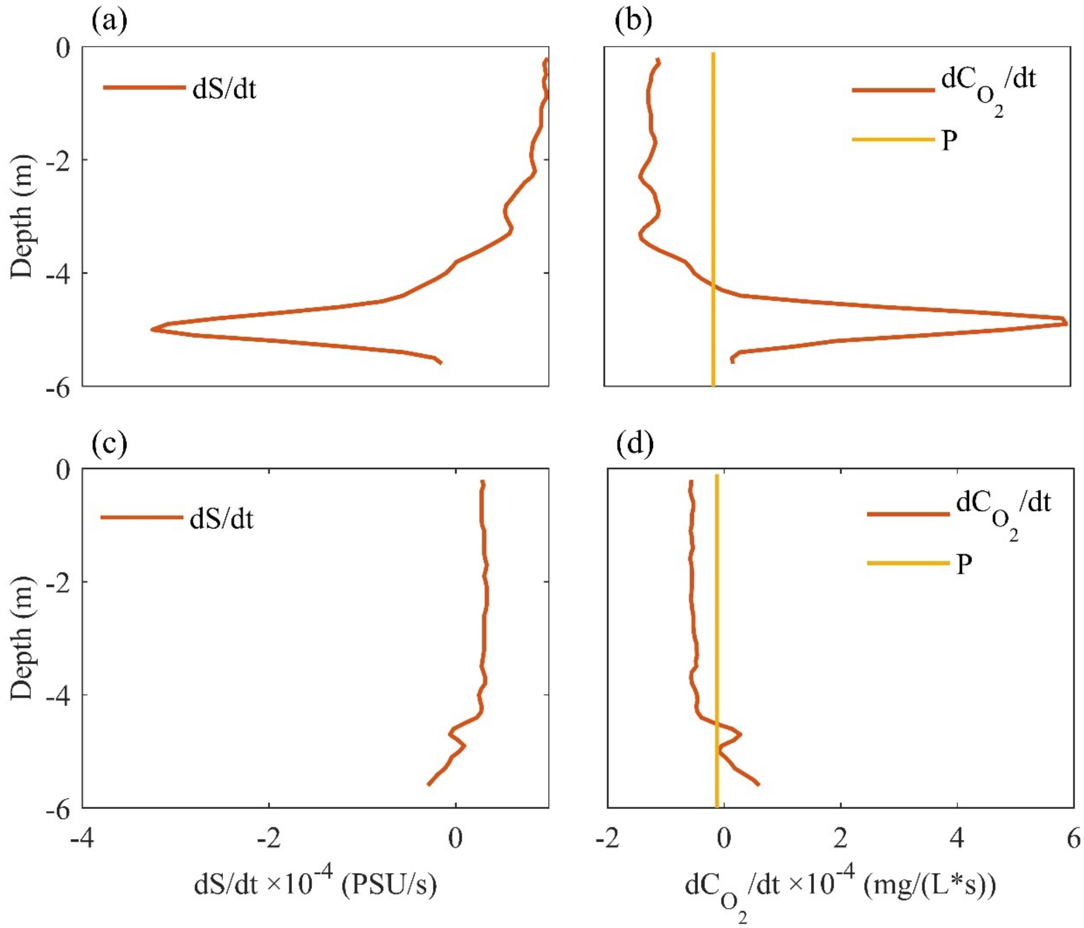

Figure 10. Vertical profiles of the (a, c) time rate of change of salinity, and (b,d) time rate of change of dissolved oxygen (red) and production and respiration (yellow) during the up-estuary wind event at (a,b) 20:00 and (c,d) 23:00 on Sept.19th.

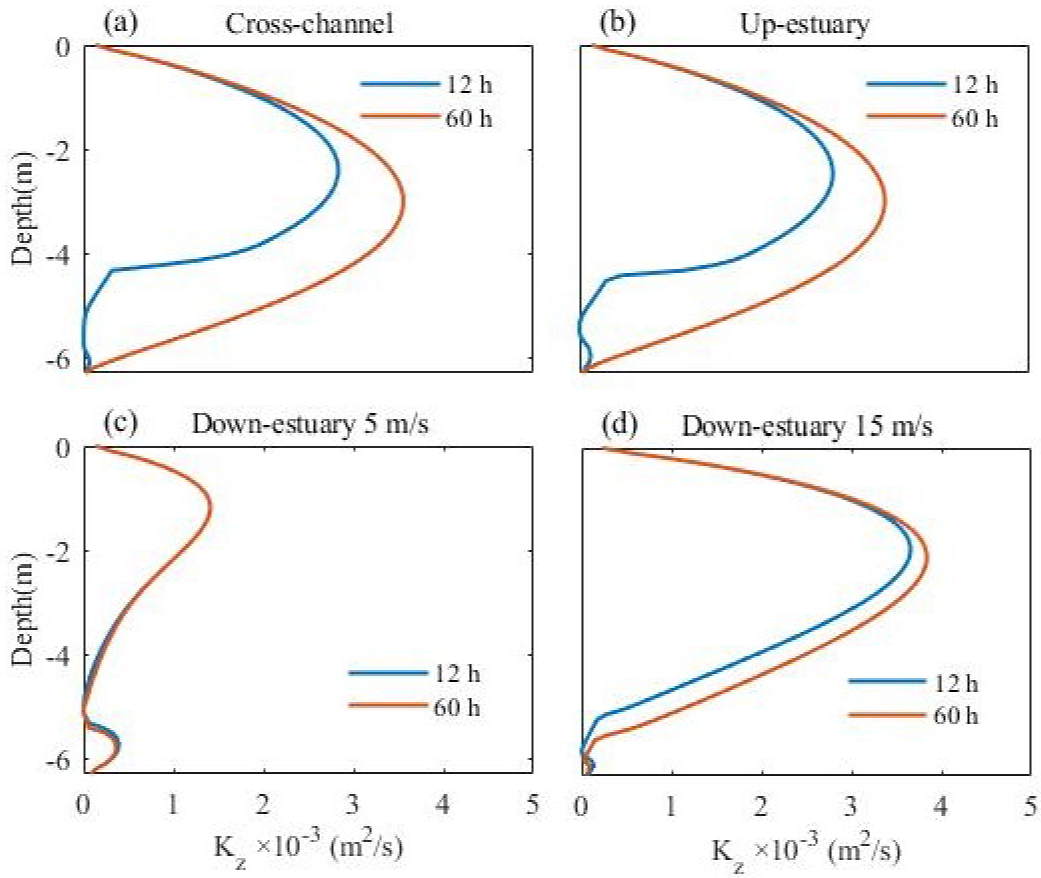

Figure 11. Vertical profiles of eddy diffusivity (K_z) from GOTM simulation after 12h (blue) and 60h (red) in a) cross-channel wind case, b) up-estuary wind case, c) 5 m/s down-estuary wind case and d) 15 m/s down-estuary wind case.

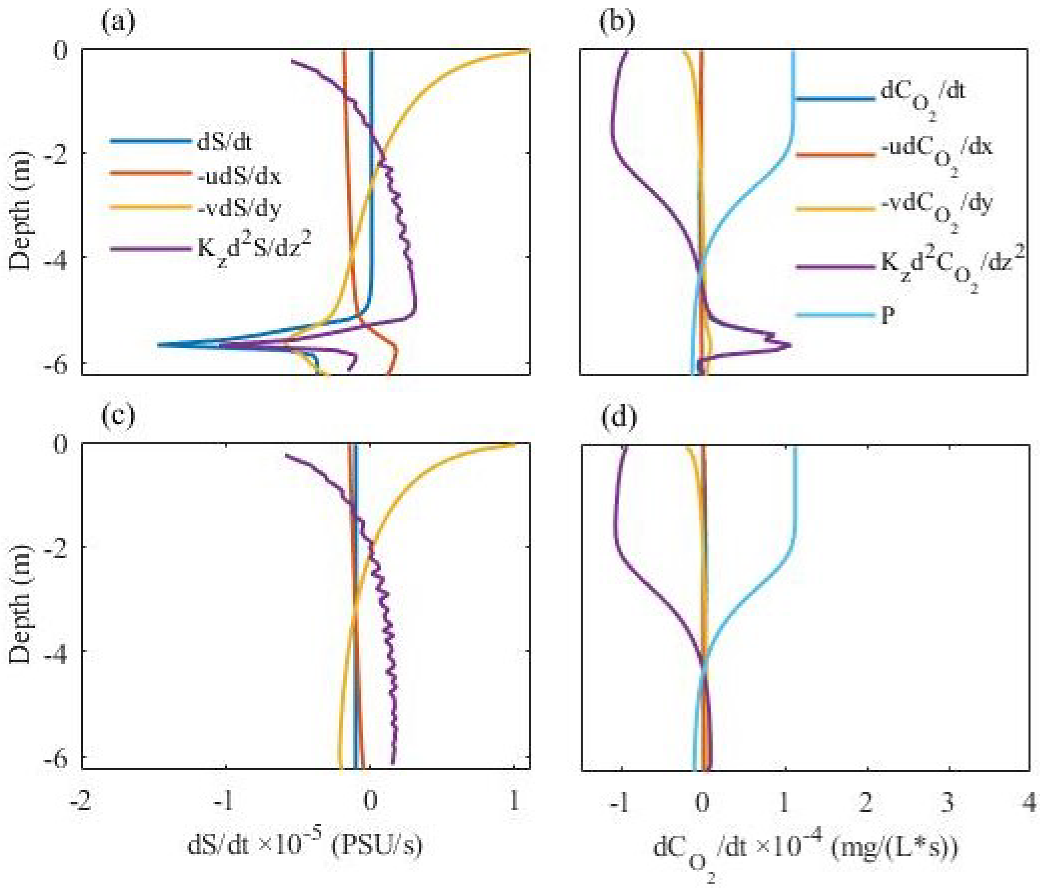

Figure 12. Vertical profiles of salinity budget terms from GOTM simulations of cross-estuary wind after a) 12 hours and c) 60 hours and dissolved oxygen budget (DO) at b) 12 hours and d) 60 hours.

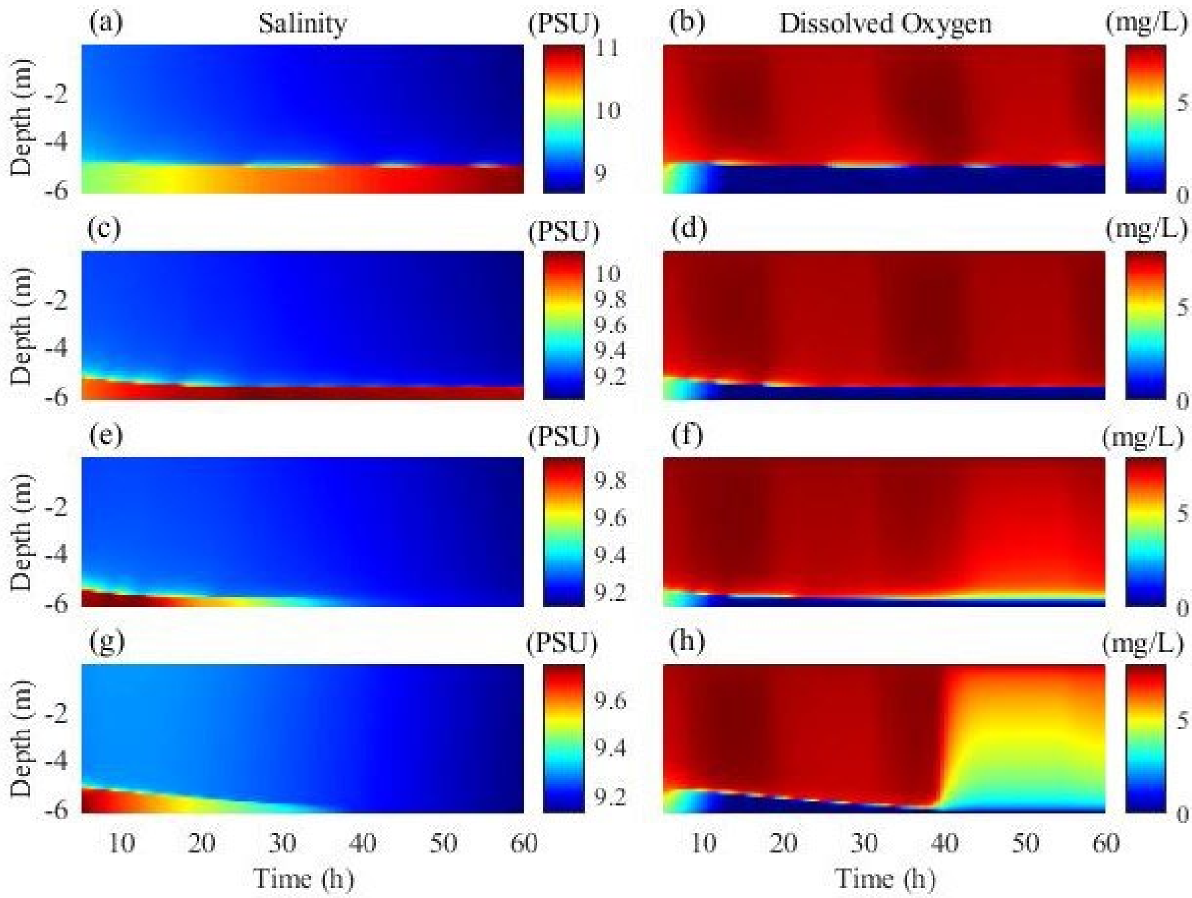

Figure 13. Time series of salinity and dissolved oxygen profiles from GOTM simulations with (a,b) 5m/s, (c,d) 10 m/s and (e,f) 15 m/s down-estuary wind and (g,h) up-estuary wind.

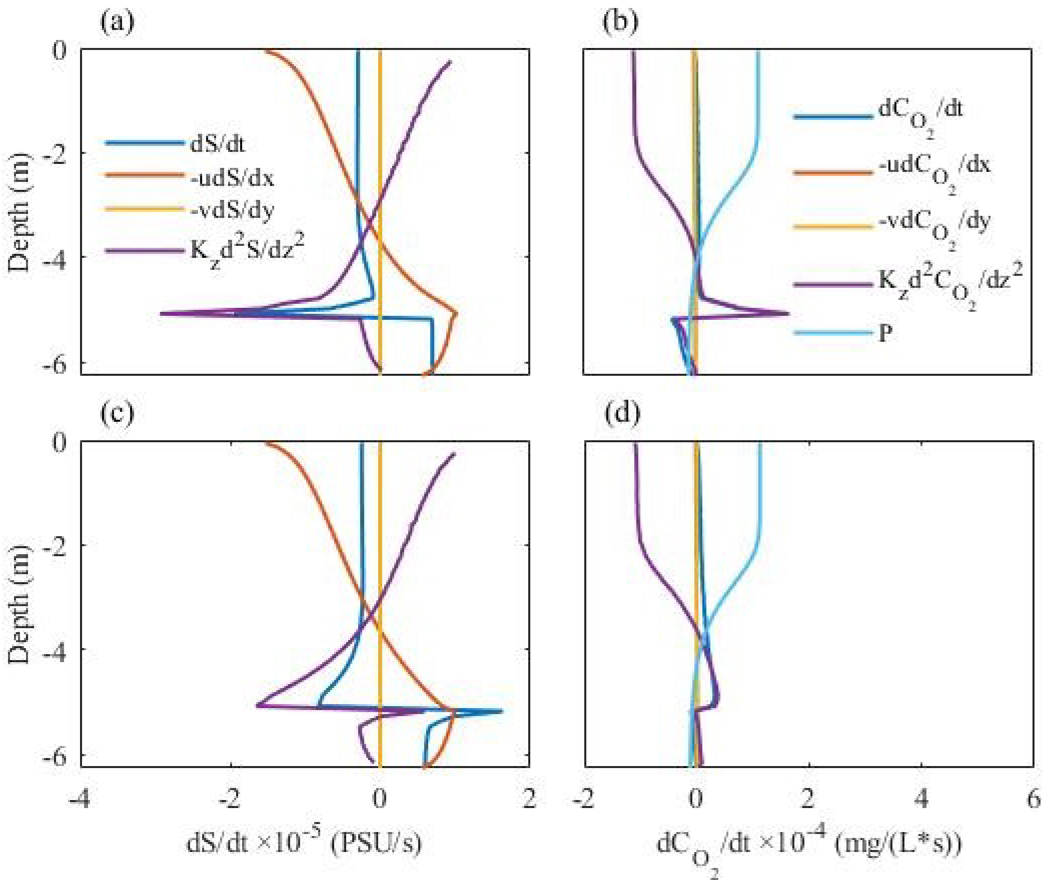

Figure 14. Vertical profiles of salinity budget terms from GOTM simulations of 5 m/s down-estuary wind after a) 12 hours and c) 60 hours and dissolved oxygen budget (DO) at b) 12 hours and d) 60 hours.

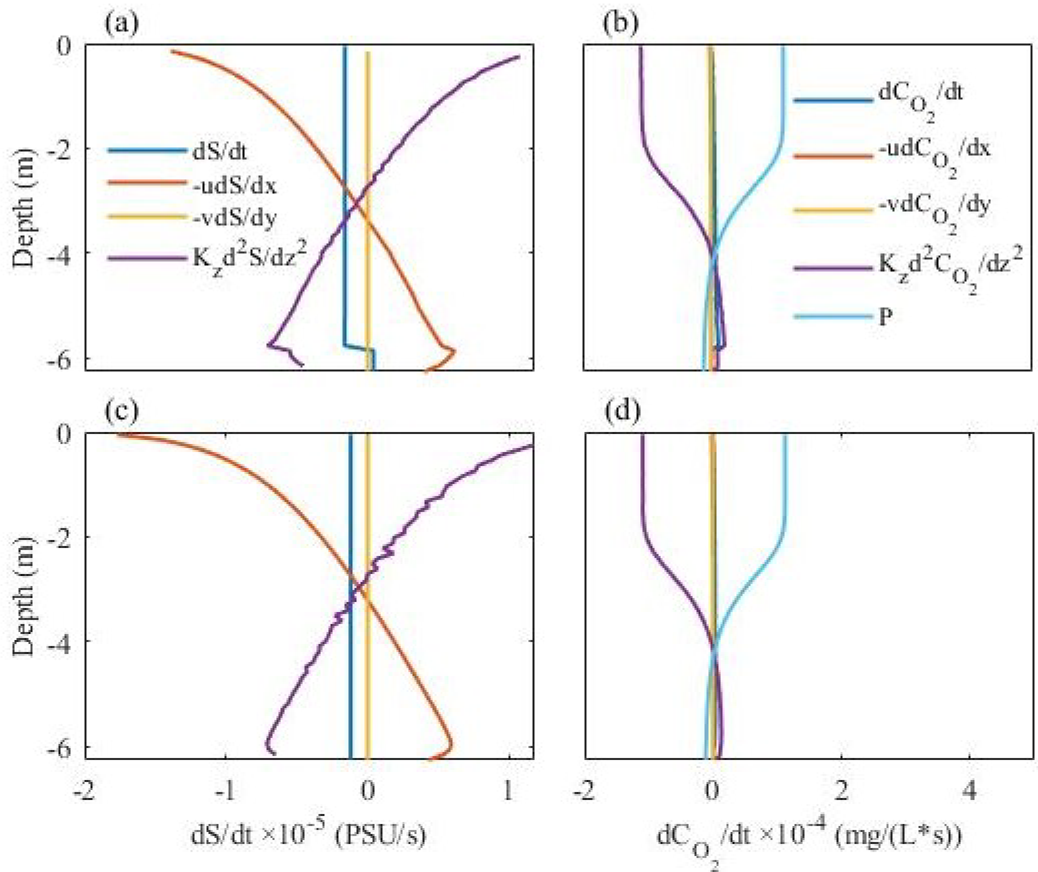

Figure 15. Vertical profiles of salinity budget (Equation 1) and dissolved oxygen budget (Equation 2) terms from idealized simulations at 1 month for (a, b) 10 m/s and 60 hours for (c, d) 15 m/s down-estuary wind scenarios.

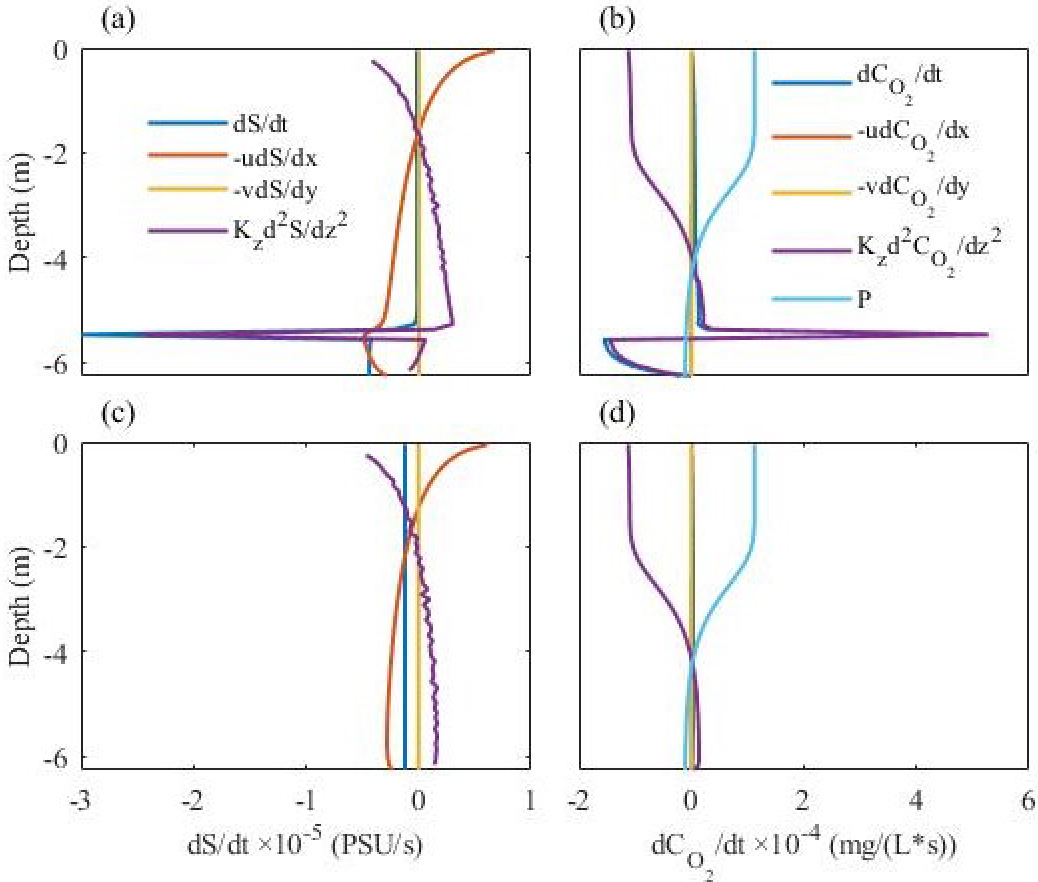

Figure 16. Vertical profiles of salinity budget terms (Equation 1) from idealized simulations of up-estuary wind at a) 12 hours and c) 60 hours and dissolved oxygen budget terms (Equation 2) at b) 12 hours and d) 60 hours.